C h a p t e r 2

FMRFAMIDE-LIKE PEPTIDES EXPAND THE BEHAVIORAL REPERTOIRE OF A DENSELY CONNECTED NERVOUS SYSTEM

Lee JS*, **Shih PY***, Schaedel ON, Quintero-Cadena P, Rogers AK and Sternberg PW (2017) FMRFamide-like peptides expand the behavioral repertoire of a densely connected nervous system. *Proceedings of the National Academy of Sciences USA* 114(50): E10726-E10735. doi: 10.1073/pnas.1710374114
*Equal contribution

2.1 Abstract

Animals, including humans, can adapt to environmental stress through phenotypic plasticity. The free-living nematode *Caenorhabditis elegans* can adapt to harsh environments by undergoing a whole-animal change, involving exiting reproductive development and entering the stress-resistant dauer larval stage. The dauer is a dispersal stage with dauer-specific behaviors for finding and stowing onto carrier animals, but how dauers acquire these behaviors, despite having a physically limited nervous system of 302 neurons, is poorly understood. We compared dauer and reproductive development using whole-animal RNA-seq at fine time points, and at sufficient depth to measure transcriptional changes within single cells. We detected 8,042 differentially expressed genes during dauer and reproductive development, and observed striking up-regulation of neuropeptide genes during dauer entry. We knocked down neuropeptide processing using *sbt-1* mutants, and demonstrate that neuropeptide signaling promotes the decision to enter dauer over reproductive development. We also demonstrate that during dauer, neuropeptides modulate the dauer-specific nictation behavior (carrier animal-hitchhiking), and is necessary for switching from repulsion to CO_2 (a carrier animal cue) in non-dauers to CO_2 attraction in dauers. We tested individual neuropeptides using CRISPR knockouts and existing strains, and demonstrate that the combined effects of *flp-10* and *flp-17* mimic the effects of *sbt-1* on nictation and CO_2 attraction. Through meta-analysis, we discovered similar up-regulation of neuropeptides in the dauer-like infective juveniles of diverse parasitic nematodes, suggesting the anti-parasitic target potential of SBT-1. Our findings reveal that under stress, increased neuropeptide signaling in *C. elegans* enhances their decision-making accuracy, and expands their behavioral repertoire.

2.2 Introduction

Stress during development can have long-lasting effects on animal physiology and behavior. For instance, trauma during early human childhood can lead to difficulties with coping against depression and anxiety in adults (1-4). Phenotypic plasticity allows animals to adapt to stresses from the environment (5). Examples of phenotypic plasticity include the production of new antibodies by the mammalian immune system (6), temperature-dependent sex determination in reptiles (7, 8), and crowding-induced cannibalism in the spadefoot toad (5, 9).

The free-living bacterivore *Caenorhabditis elegans* can adapt to stressful conditions by exiting reproductive development and entering the stress-resistant dauer larval stage (10-12). In reproductive development, *C. elegans* develops through four larval stages (L1, L2, L3, and L4) to become a reproductive adult. Declining food, temperature, and crowding conditions, however, promote L1 entry into pre-dauer L2d. If conditions improve, L2d commit to reproductive development through amplification of dafachronic acid growth hormone across the animal body (13). Unimproved conditions cause L2d to commit to dauer development, through a process that is not well understood. Following this event, L2d larvae molt into dauer larvae and halt their feeding.

Dauers are less metabolically active than non-dauers, and can survive long periods of starvation by utilizing stored lipids, in lieu of aerobic respiration (14, 15). Morphologically, they have a highly impermeable cuticle that allows them to resist environmental assaults (10). In addition, they have a rewired nervous system (16, 17), and specialized dispersal behaviors for finding and stowing onto carrier animals (18, 19).

Dauer lifespans are ten times longer than those of non-dauers (20), and dauers can resume reproductive development with an unaffected adult lifespan once they recover under favorable conditions (21). Thus, dauers have much to reveal about the biological control of longevity, stress-resistance, and neural state.

The genetic and anatomical tractability of *C. elegans* make it an advantageous model for studying phenotypic plasticity in a whole organism. Previous systems-level studies have analyzed the *C. elegans* transcriptome during molt into dauer, during dauer, and during recovery from dauer (22-24). However, the transcriptome of L2d during the dauer entry decision has not been characterized, likely because L2d lack strong distinguishing traits that can be used to isolate them (25). Furthermore, dauer and reproductive development have not been compared under parallel growth conditions, which has limited the discovery of genes that are differentially expressed between the two developments.

Therefore, we have used techniques from our previous analysis of *daf-9(dh6)* loss-of-function animals (13) to add crucial detail to dauer development. Using dafachronic acid, we controlled the developmental decisions of *daf-9(dh6)* L2d, under parallel conditions. We coupled this with our previous timing of *daf-9(dh6)* development to collect pure populations of uncommitted L2d, dauer-committed L2d, L3-committing L2d, dauers, and L4. We performed whole-animal RNA-seq on these populations, revealing 8,042 differentially expressed genes during dauer and reproductive development. Through enrichment analysis, we observed striking up-regulation of neuropeptide genes during dauer-commitment. Using the *sbt-1(ok901)* null mutant to knock down neuropeptide processing (26), we demonstrate that peptidergic signaling promotes the dauer entry

decision, promotes coordination during nictation (a hitchhiking behavior), and is necessary for switching from CO_2 repulsion in non-dauers to CO_2 attraction in dauers.

Testing individual neuropeptides using CRISPR knockouts and existing strains, we demonstrate uncoordinated nictation and CO_2 avoidance phenotypes in *flp-10(n4543) flp-17(n4894)* double mutants, similar to *sbt-1(ok901)*. Through a meta-analysis, we discovered similar up-regulation of neuropeptides in the dauer-like infective juveniles of diverse parasitic nematodes, suggesting the anti-parasitic target potential of SBT-1. Our results reveal that the *C. elegans* nervous system responds to environmental stress by increasing neuropeptide signaling to enhance decision-making, and to enable specialized dispersal behaviors. The expansion of the neuropeptide genes, especially the FMRFamide-like neuropeptide (*flp*) genes, in nematodes has been a puzzle (27, 28), and our results provide one reasonable explanation.

2.3 Results

RNA-seq was used to investigate dauer and reproductive development

Our previous analysis of the *daf-9(dh6)* null mutant in (13) allowed us to sequence cDNA from large quantities of dauer- and reproductive-developing animals. Briefly, *C. elegans* DAF-9 is a cytochrome P450 enzyme that synthesizes the growth hormone dafachronic acid (DA) (29, 30). Commitment to reproductive development only occurs when the level of DA in the animal body is high enough to trigger feedback amplification of DA across the entire organism, thus locking the developmental decision (13). *daf-9(dh6)* null mutants cannot produce their own DA, and therefore constitutively form dauers unless synthetic DA is added to induce reproductive development (13, 30, 31). We previously characterized the timing of development in *daf-9(dh6)* animals: dauer-commitment occurs at 33 hours post hatch (hph), followed by molt into dauer at 48 hph (13). However, if DA is added at 24 hph, *daf-9(dh6)* L2d commit to reproductive development by 27 hph, and molt into L4 at 34 hph.

Using these conditions, we grew synchronized populations of dauer-developing *daf-9(dh6)* by withholding synthetic DA, and we collected L2d animals (at 24 hph and 26 hph), dauer-committed L2d (at 34 hph), and fully developed dauers (at 60 hph) for RNA sequencing (**Figure 2.1A**). In parallel, we added synthetic DA to a sub-culture, forcing it into reproductive development, and from which we collected L3-committing larvae (at 26 hph) and L4 (at 34 hph) for sequencing. We sequenced each sample using two biological replicates, at an average depth of 100 million reads (the sum of the replicates) (**Appendix Table 2.1**). Since *C. elegans* animals contain 959 cells (32), and each cell likely expresses

100,000 mRNA transcripts (33, 34), we estimated that we had sequenced one read for every transcript in the whole animal at each time point. Therefore, we expected to detect signals from transcripts as long as they were not expressed in few cells at low abundance. For each sample, we detected between 20,519 to 22,672 expressed genes, of the total 20,362 coding and 24,719 non-coding genes of the *C. elegans* genome (35, 36) (**Figure 2.2A** and **Appendix Table 2.2**).

PCA analysis revealed the extent of variation between developmental stages

We analyzed the variation between our transcriptomes using principal component analysis (PCA) (**Figure 2.2B-C**). Replicate samples had similar PC scores to each other, indicating that our biological replicates were well correlated in their gene expression. Our analysis also revealed that the largest sources of variation between our transcriptomes were the differences between dauer-commitment/differentiation versus the remaining time points (principal component 1, 65% of overall variation), and the difference between 24 hph L2d and 26 hph L2d (principal component 2, 17% of overall variation). Along the first two principal components, 24 hph L2d and L4 demonstrated close similarity, as did 26 hph L2d and L3-committing larvae, as well as dauer and dauer-committed larvae.

8,042 genes are differentially expressed during dauer and reproductive development

Using the differential gene expression analysis program DESeq (37, 38), we performed pairwise comparisons between 24 hph L2d and 26 hph L2d to identify gene expression changes during L2d sensory integration; between L2d and dauer-committed larvae for changes during dauer-commitment; and between L2d and dauer larvae for changes during

differentiation and maintenance of dauer (**Figure 2.1B**). With our reproductive development samples, we performed pairwise comparisons between L2d and L3-committing larvae for changes during commitment to reproductive development, and between L2d and L4 for changes during reproductive growth. In addition, our design allowed us to perform pairwise comparisons between age-matched dauer- and reproductive-developing animals at 26 hph (L2d versus L3-committing larvae) and 34 hph (dauer-committed larvae versus L4) to identify gene expression changes specific to one developmental track (**Figure 2.1C**). We avoided sequencing an age-matched reproductive sample for 60 hph dauer since reproductive animals at 60 hph are gravid and inappropriate for studying a stage-specific transcriptome. In total, we performed twelve pairwise comparisons between our dauer and reproductive time points. In each comparison, we detected between 484 to 2,276 up-regulated genes, and 280 to 2,824 down-regulated genes (**Figure 2.1D** and **Appendix Table 3**). Overall, we observed 8,042 differentially expressed genes from the twelve comparisons. These genes corresponded to 7,866 coding genes and 77 ncRNA genes, indicating that 39% of the *C. elegans* protein-coding genome is differentially expressed during dauer and reproductive development.

Differential expression was detected at high accuracy and single-cell resolution

To analyze the resolution of our RNA-seq dataset, we used WormBase anatomical-level gene expression data to search our 8,042 differentially expressed genes for genes previously reported to have tissue-specific expression. We detected transcriptional changes in 47 epithelial system genes (of 74 total epithelium-specific genes in WormBase), 56 muscular system genes (of 89 total), 181 alimentary system genes (of 310 total), 108

reproductive system genes (of 233 total), 139 nervous system genes (of 599 total), 9 amphid sensillum genes (of 62 total), and 1 XXX cell gene (of 4 total) (**Figure 2.3A**). This analysis suggests that we could detect differential expression from within tissues and single cells. Indeed, we constructed fluorescent transcriptional reporters for *col-40* and *srt-41*, which were up-regulated in our data during dauer development, and we observed previously unreported, specific expression for the two genes in the hypodermis and the AWC neuron, respectively (**Figure 2.3B-O**).

We examined the accuracy of our dataset by comparing to SAGE data published by Jones, *et al*. (2001), and microarray data published by Wang & Kim (2003), which have identified genes that are enriched in wild type dauers versus mixed-populations or post-dauer adults, respectively (24, 39). When tested for differential expression in our data, 141 (45%) of the dauer-enriched genes from (39) were significantly up-regulated at dauer-commitment and dauer, relative to L2d and L4 (**Figure 2.3P**). Similarly, 312 (69%) of the dauer-enriched genes from (24) were significantly up-regulated at dauer-commitment and dauer. Thus, our calculations for differential expression (negative binomial testing at a Benjamini-Hochberg controlled false discovery rate < 0.01) may have been more stringent than the calculations in (24, 39). Other differences may be explained by gene expression changes that are only observable between dauer and post-dauer, and by differences in the *daf-9(dh6)* strain we used versus the wild type strain. Nonetheless, we conclude from this analysis that *daf-9(dh6)* and wild type transcriptomes demonstrate high comparability, and that our differential expression testing is conservative.

Clustering revealed six common expression profiles during dauer and reproductive development

Soft clustering is a sensitive method for identifying common expression profiles within a dataset (40, 41). We performed soft clustering on our 8,042 differentially expressed genes to group the genes by similarities in their expression profiles. This revealed six clusters (clusters 1-6), indicating that differential gene expression through dauer and reproductive development can be described by six common expression profiles (**Figure 2.4**): the expression levels of 1,102 genes gradually decreased into dauer (cluster 1), 1,921 genes gradually increased into dauer (cluster 2), 1,025 genes increased transiently at 26 hph (cluster 3), 1,497 genes increased transiently during dauer-commitment (cluster 4), 1,332 genes decreased after dauer-commitment (cluster 5), and 1,165 genes increased in L4 (cluster 6) (**Appendix Table 2.4**).

The genes from clusters 2 and 4 encompass 3,418 genes likely involved in commitment, differentiation, and maintenance of dauer. These highly dauer-specific genes represent a 7.6-fold expansion over the 449 'dauer-enriched' genes described previously (24). In addition, the genes from clusters 1, 3, 5, and 6 encompass 4,624 genes whose expressions are largely excluded during dauer-commitment and dauer.

We examined the six clusters for enriched biochemical pathways and gene ontology (GO) terms using KEGG biochemical pathway data (42-44), and the PANTHER Classification System (45). We observed that cluster 1 (genes with decreasing expression into dauer) was enriched for the "peroxisome" KEGG pathway, suggesting that peroxisomal activity is reduced in dauers (**Figure 2.4**). This is consistent with the reduction of ascarocide pheromone production in dauers (46), since a key step of ascarocide

biosynthesis occurs via peroxisomal β-oxidation (47). In fact, cluster 1 contains genes for the β-oxidation enzymes ACOX-1, MAOC-1, and DHS-28, which perform 3 of the 4 steps of ascarocide side chain biosynthesis (47).

Cluster 2 (genes with increasing expression into dauer) was enriched for the "FoxO signaling pathway" and "longevity regulating pathway – worm" KEGG pathways, as may be expected from the extended longevity of dauers (20), and the role of FOXO signaling in modulating longevity and stress resistance (11) (**Figure 2.4** and **Appendix Table 2.4**). We observed 13 members (18%) of the "longevity regulating pathway – worm" in cluster 2, including members in the branches of the pathway that respond to environmental cues, dietary restriction, oxidative stress, germline state, and the mitochondrial unfolded protein response to affect lifespan (42-44). The remaining input into the longevity regulating pathway, the hypoxia branch, did not have any members in cluster 2. This suggests the intriguing possibility that the extreme longevity of dauer arises from the simultaneously enhanced activity of five of the six branches of the longevity pathway.

We also observed enrichment of the "neuropeptide signaling pathway" GO term in cluster 2 (**Figure 2.4**), suggesting that neuropeptides modulate the dauer-commitment decision and/or neural functions downstream of the decision. Indeed, some neuropeptides have been shown to affect dauer biology: insulin signaling via DAF-28, INS-4, and INS-6 promotes reproductive growth over dauer development, and INS-1 and INS-18 antagonize this pathway (reviewed in (48)). In addition, FMRFamide signaling via FLP-18 acts in parallel with the TGF-β signaling pathway to inhibit dauer development (49). Furthermore, *ins-3*, *6*, *18*, *20*, *27-28*, *31*, *34*, and *daf-28* have been shown to affect the fraction of time that is spent nictating in dauer (50).

In cluster 3 (genes with increased expression at 26 hph), we observed enrichment for biomolecule synthesis and turnover pathways, including the "proteasome," "lysosome," "fatty acid degradation," and "fatty acid elongation" KEGG pathways (**Figure 2.4**, **Figure 2.5**, and **Appendix Table 2.4**). This observation may reflect the developmental uncertainty in L2d, and perhaps represents a bet-hedging strategy of cycling biomolecules in preparation for either commitment decision. Consistent with the prediction of developmental uncertainty, genes with the "molting cycle" GO term were enriched (2.9-fold enrichment, $p = 2.54 \times 10^{-14}$) among the genes up-regulated in 26 hph L2d versus 24 hph L2d (**Appendix Table 2.3**), despite molt into dauer, one of the two possible molts from L2d, occurring 22 hours later at 48 hph.

In cluster 4 (genes with increased expression at dauer-commitment), we observed enrichment of the "neuroactive ligand-receptor interaction" and "calcium signaling pathway" KEGG pathways (**Figure 2.4**, **Figure 2.5**, and **Appendix Table 2.4**). Together with cluster 2, this indicates that several genes with neuronal functions have increased expression during dauer-commitment and dauer.

Genes that are down-regulated during dauer-commitment are likely repressed to exclude non-dauer physiologies, and indeed, our enrichment data for cluster 5 (genes with decreased expression after dauer-commitment) are consistent with the reduction of TCA cycle activity in favor of long-term lipid metabolism in dauer (51), as we observed enrichment of the "fatty acid degradation" and "citrate cycle (TCA cycle)" KEGG pathways (**Figure 2.5** and **Appendix Table 2.4**).

Cluster 6 (genes with increased expression at L4) was enriched for terms related to translation and respiration, including the "mitochondrial electron transport, ubiquinol to

cytochrome c" GO term and the "ribosome" KEGG pathway (**Figure 2.4**), which likely reflects growth during reproductive development and gametogenesis in the L4 (52-54).

Differential expression of the neuronal genome during dauer development

Our KEGG and GO enrichment analyses indicated the strong involvement of neuronal effector genes during dauer-commitment and dauer. To investigate this further, we examined the expression of the neuronal genome of *C. elegans* during dauer and reproductive development. The neuronal genome of *C. elegans* encodes 3,114 genes from 30 gene classes, including the calcium channels, neurotransmitters, G protein-coupled receptors (GPCRs), and CO_2 receptors (55). We detected the differential expression of 606 neuronal genes during dauer and reproductive development, corresponding to 19% of the total neuronal genome, with members from all of the 30 gene classes (**Figure 2.6**).

Five gene classes were enriched in one of the soft clusters 1 to 6, indicating that for these classes, a high proportion of their members followed a certain expression profile during dauer and reproductive development (**Appendix Table 2.5**). The extracellular immunoglobulin and leucine rich repeat domain gene class was over-represented in cluster 1 (decreasing expression into dauer), with 2.8-fold enrichment and $p = 6.42 \times 10^{-3}$. The neuropeptide gene class was over-represented in cluster 2 (increasing expression into dauer), with 3.1-FE and $p = 6.32 \times 10^{-21}$. Finally, the GPCR (2.9-FE, $p = 2.41 \times 10^{-8}$), CO_2 and O_2 receptor (4.9-FE, $p = 7.86 \times 10^{-5}$), and potassium channel gene classes (3.0-FE, $p = 2.84 \times 10^{-3}$) were over-represented in cluster 4 (increased expression at dauer-commitment).

GPCR gene expression increases sharply during dauer-commitment, before neuropeptide gene expression reaches its peak during dauer (**Figure 2.6**). In addition, the 34 GPCRs in cluster 4 include 1 biochemically de-orphanized neuropeptide GPCR (*npr-11*) and 9 putative neuropeptide GPCRs (*ckr-1*, *frpr-7*, *-19*, *npr-17*, *-31*, C01F1.4, F13H6.5, Y37E11AL.1, and Y70D2A.1) (27, 55) (**Appendix Table 2.5**). This suggests that neuropeptide receptors are up-regulated during dauer-commitment in anticipation of increasing neuropeptide gene expression during dauer-commitment and dauer.

Notably, the neuropeptide gene class was the only class that was enriched for increasing expression into dauer. We observed extensive up-regulation of the neuropeptides during dauer development: in dauer-commitment (34 hph) versus L2d (24 hph), 60 of the 118 total neuropeptide genes were up-regulated while 9 were down-regulated (**Figure 2.9A**). Similarly, at dauer-commitment (34 hph) versus L4 (34 hph), 43 neuropeptide genes were up-regulated while 10 were down-regulated (**Figure 2.10A**), and in dauer (60 hph) versus L2d (24 hph), 64 neuropeptide genes were up-regulated while 9 were down-regulated (**Figure 2.10B**). The up-regulation of 64 neuropeptide genes during dauer versus L2d is remarkable, as it corresponds to the majority of all neuropeptide genes in the *C. elegans* genome. Furthermore, the 64 genes encode for 215 putative or biochemically isolated peptides (48). By comparison, the human genome contains a total of 97 neuropeptide genes that encode for 270 peptides (56).

Peptidergic signaling downstream of SBT-1 promotes dauer entry and nictation coordination, and is necessary for CO_2 chemoattraction in dauer

Neuropeptides become functional transmitters and neuromodulators only after they are cleaved from longer proneuropeptide chains (48) (**Figure 2.8A**). SBT-1/7B2 is a chaperone for the proprotein convertase EGL-3/PC2, which cleaves proneuropeptides (57), and as a result, *sbt-1*(*ok901*) null mutants have reduced levels of mature neuropeptides compared to wild type (26) (**Figure 2.8B**). Previously, *sbt-1*(*ok901*) mutants were reported to possess aldicarb resistance and extended lifespans (58, 59), but to our knowledge, no functions for *sbt-1* in dauer biology have been reported.

Because we observed up-regulation of neuropeptides starting from dauer commitment, we tested the ability of *sbt-1*(*ok901*) mutants to enter dauer, using crude pheromone to induce dauer entry. Under the same dauer-inducing conditions, wild type animals entered dauer 49% of the time, while *sbt-1*(*ok901*) mutants entered dauer 16.5% of the time (**Figure 2.8C**). We also observed that expressing *sbt-1* genomic DNA in *sbt-1(ok901)* mutants (under the control of the endogenous promoter) rescued the dauer entry phenotype in two independent lines: rescue line 1 entered dauer 46% of the time, and rescue line 2 entered dauer 37% of the time (**Figure 2.8C**). These results suggest that the net effect of peptidergic signaling downstream of SBT-1 promotes dauer entry over reproductive development.

We examined if neuropeptides play a role during dauer, when the majority of the *C. elegans* neuropeptide genes were expressed the highest in our dataset. *C. elegans* dauers have been found to associate with invertebrate carriers, likely for transportation to new niches (60). Nictation, where dauers stand on their tail and wave their body, and CO_2 chemoattraction are two dauer-specific behaviors that likely enable dauers to migrate toward and attach onto carriers (18, 61). We tested *sbt-1*(*ok901*) nictation on micro-dirt

chips, which provide substrates for dauers to nictate on, and observed that the average nictation duration doubled in *sbt-1(ok901)* mutants (μ = 28.90 seconds, max = 139.63 seconds) as compared to wild type (μ = 14.44 s, max = 32.32 s). Moreover, the phenotype was rescued by *sbt-1* genomic DNA expression under the endogenous promoter (line 1: μ = 14.35 s and max = 78.00 s, line 2: μ = 14.50 s and max = 52.27 s) (**Figure 2.8D**). We observed a difference in the degree of three-dimensional movement during nictation in wild type and *sbt-1(ok901)* mutant animals that may explain the increased duration of nictation in *sbt-1(ok901)* mutants: while wild type animals displayed a wide range of motion and fell back to the chip easily, *sbt-1(ok901)* animals displayed a limited range of motion and slow, uncoordinated waving that likely increased stability during nictation (**Appendix Video 2.1** and **2.2**). We did not observe significant differences in other components of the nictation behavior, such as initiation frequency and the proportion of time spent nictating (19) (**Figure 2.7A-B)**.

CO_2 has been shown to be attractive to dauers and replusive to non-dauers (18, 62). Using chemotaxis assays, we observed attraction to CO_2 in wild type dauers (chemotaxis index = 0.59) and repulsion to CO_2 in *sbt-1(ok901)* dauers (chemotaxis index = -0.53) (**Figure 2.8E**). We further performed CO_2 acute avoidance assays by delivering CO_2 directly to the nose of forward-moving dauers and scoring reversal. While wild type dauers did not avoid CO_2 (avoidance index = -0.11), we observed rapid reversal in *sbt-1(ok901)* mutants in response to CO_2 (avoidance index = 0.64). In addition, the CO_2 repulsion phenotype of *sbt-1(ok901)* was rescued by *sbt-1* genomic DNA (line 1: avoidance index = 0.04, line 2: avoidance index = 0.06) (**Figure 2.8F** and **Appendix Video 2.3-2.6**). Together, our results indicate that the neuropeptides downstream of SBT-1 modulate

proper nictation coordination, and are necessary for the correct CO_2 preference switch from aversion in non-dauers to attraction in dauers. To our knowledge, we have reported for the first time the genetic control of the CO_2 preference switch in dauer.

The 31-gene *flp* family is coordinately up-regulated during dauer development

The *C. elegans* genome encodes for three families of neuropeptides: the FMRFamide-like peptides (31 *flp* genes), the insulin related peptides (40 *ins* genes) and the neuropeptide-like proteins (47 *nlp* genes) (48). In dauer-commitment versus L2d, we observed the up-regulation of almost all of the *flp* genes, with significant increases in expression for *flp-1-2*, *4-9*, *11-22*, *24-28*, and *32-34* (28 of 31 total) (**Figure 2.9A** and **Appendix Table 2.3**). In contrast, a smaller proportion of *ins* and *nlp* genes were up-regulated during dauer-commitment versus L2d: *ins-1*, *17-18*, *24*, *28*, *30*, and *daf-28* (7 of 40 total); and *nlp-1-3*, *6*, *8-15*, *17-18*, *21*, *35*, *37-38*, *40-42*, *47*, *ntc-1*, *pdf-1*, and *snet-1* (25 of 47). Similar results were observed during dauer-commitment versus L4 (**Figure 2.10A**), and dauer versus L2d (**Figure 2.10B**). Therefore, the *flp* genes, more than the *ins* or *nlp* genes, are coordinately up-regulated during dauer development.

We quantified this coordination in *flp* gene expression by pairing every combination of the 31 *flp* genes and scoring the correlation between the expression of each pair of genes across our RNA-seq dataset. The average correlation score between the *flp* genes was 0.88, with possible scores ranging from -1 (perfectly anti-correlated) to 1 (perfectly correlated) (**Figure 2.9B**). By comparison, the average correlation scores for random sets of 31 genes (mimicking the size of the *flp* family) were distributed around a bootstrapped mean of 0.02. In addition, the *ins* and *nlp* genes had an average score of 0.21 and 0.28, respectively.

Furthermore, we obtained similar results when we expanded our correlation analysis to include expression data from 246 publically available RNA-seq datasets describing a broad range of *C. elegans* life stages and experimental conditions (23) (**Figure 2.10C-D**). Using dotplot analysis (63), we examined whether the 31 *flp* genes share regions of sequence similarity (**Figure 2.10E**). We observed that there are no regions of shared sequence among the *flp* genes that extends beyond 20 nucleotides, with only two regions sharing a 20-nucleotide match (between *flp-2* and *flp-22*, and between *flp-27* and *flp-28*). Therefore, it is unlikely that the high correlation between *flp* gene expressions was caused by any cross-mapping of RNA-seq reads among the 31 *flp* genes, since our sequenced reads were 50 to 100 base pairs in length. Together, these results strongly suggest that the *flp* genes are co-regulated and are coordinately up-regulated during dauer development.

FLPs modulate the dauer entry decision, nictation, and CO_2 chemoattraction

We investigated whether FLP neuropeptides modulate the dauer entry decision by assaying 4 CRISPR-generated knockout alleles and 19 available *flp* alleles, corresponding to mutations in 18 *flp* genes. We induced dauer entry using crude pheromone and compared the dauer entry percentage of each genotype to the wild type control. We recapitulated the previously reported increased dauer entry phenotype of *flp-18(db99)* as a positive control (49). We observed increased dauer entry in three additional *flp* mutants: *flp-2(ok3351)*, *flp-6(ok3056)*, and *flp-34(sy810)*. Furthermore, we detected decreased dauer entry in 8 mutants: *flp-1(yn4)*, *flp-8(pk360)*, *flp-10(ok2624)*, *flp-11(tm2706)*, *flp-17(n4894)*, *flp-21(pk1601)*, *flp-25(gk1016)*, and *flp-26(gk3015)* (**Figure 2.9C**). These results suggest that FLPs can act redundantly and with opposed effects on dauer entry.

flp-10 and *flp-17* are expressed in the CO_2 sensing BAG neuron (64, 65), and act synergistically with the neurotransmitter acetylcholine, which promotes the nictation behavior (19), to inhibit egg-laying (66). Because of these connections to nictation and CO_2-sensing, we examined nictation and CO_2 chemoattraction in *flp-10(n4543) flp-17(n4894)* double mutant animals. Using the micro-dirt chip, we observed an average nictation duration of 14.44 seconds for wild type, and an increased average duration of 25.02 seconds in *flp-10(n4543) flp-17(n4894)* mutants (**Figure 2.9D**). For CO_2 avoidance, we observed that *flp-10(n4543) flp-17(n4894)* mutants displayed increased reversal behavior in response to CO_2 (avoidance index = 0.56) as compared to wild type (avoidance index = -0.11) (**Figure 2.9E**). These data suggest that *flp-10* and *flp-17* contribute to SBT-1 functions in mediating nictation coordination and the switch to CO_2 attraction in dauers.

flp genes are coordinately up-regulated in parasitic nematode IJs

The infective juvenile (IJ) dispersal stage of parasitic nematodes is similar to dauer in several ways: both are non-feeding stages with a resistant cuticle (67), and both recognize and exploit carriers/hosts similarly (18, 68). One gene class that has been shown to affect dauers and IJs is the neuropeptide-encoding set of genes (27, 48). To investigate if the coordinated up-regulation of *flp* genes is a strategy shared by dauers and IJs, we performed a meta-analysis on *flp* gene expression in IJs of the semi-obligate animal parasite *Strongyloides stercoralis*, the obligate animal parasite *Ancylostoma ceylanicum*, the obligate plant parasite *Globodera pallida*, and the filarial parasite *Brugia malayi*. We selected these distantly related parasitic species because the orthologs/analogs of *C. elegans flp* genes have been identified in these nematodes (69). In addition, the transcriptomes of

these species had been collected using RNA-seq, from stages during, before, and after IJ (70-73).

There are 21 *flp* genes in *S. stercoralis*, 25 in *A. ceylanicum*, 14 in *G. pallida*, and 13 in *B. malayi*. We observed that each *flp* gene was expressed at its highest level during the IJ or post-infection IJ in *S. stercoralis*, *A. ceylanicum*, and *G. pallida*, and was expressed lowly in other stages, including the egg, the first larval, third larval, fourth larval, and adult stages (**Figure 2.11B-D**). Specifically, *S. stercoralis* expressed 16 *flp* genes highly in IJ, and 5 highly in the post-infection IJ (**Figure 2.11B**); *A. ceylanicum* expressed 18 *flp* genes highly in IJ, and 5 highly in the post-infection IJ (**Figure 2.11C**); and *G. pallida* expressed 14 *flp* genes highly in IJ (**Figure 2.11D**).

By contrast, only 4 of the 13 *flp* genes in *B. malayi* were expressed at high levels in the IJ. The expressions of the remaining *flp* genes were specialized to other stages, such as the microfilariae and the adult male (**Figure 2.11E**). Unlike the other three parasitic nematodes, *B. malayi* spends its life cycle entirely within its hosts. Notably, the IJs of *B. malayi* infect humans through the aid of a mosquito vector (74). This differs from the IJs of *S. stercoralis*, *A. ceylanicum*, and *G. pallida*, which must find and infect their hosts (**Figure 2.11**). We therefore observe that *C. elegans* dauers and the host-seeking IJs of *S. stercoralis*, *A. ceylanicum*, and *G. pallida* share a strategy of coordinately up-regulating the *flp* family.

2.4 Discussion

In the wild, *Caenorhabditis elegans* feeds on transient microbial communities that collapse approximately every three generations (75). To persist, *C. elegans* can enter the stress-resistant dauer larval stage, which can seek improved conditions by stowing onto carrier animals (60). We sequenced cDNA from dauer- and reproductively-developing animals by culturing *daf-9*(*dh6*) animals under identical conditions apart from exposure to DA. This allowed us to collect the first transcriptomes, to our knowledge, of L2d during dauer-commitment and commitment to reproductive development. Our design also allowed us to compare dauer and reproductive development to identify gene expression changes along, and between, the two tracks. We have demonstrated that 8,042 genes are differentially expressed during dauer and reproductive development, including the up-regulation of 51% of the neuropeptide genes during dauer-commitment.

Neuropeptides are short sequences of amino acids that are derived from longer proneuropeptide chains, and can act as transmitters and neuromodulators. As neuromodulators, they can control the activity, polarity, sensitivity, and signaling repertoire of neurons (76, 77). Neuropeptides can also diffuse to facilitate signaling between synaptically unconnected neurons (78, 79). Through these modulatory functions, neuropeptides can shape which circuits are active in the nervous system, the membership of these circuits, and their functions (79).

C. elegans encodes three families of neuropeptides: the insulin-like peptides (INS), the neuropeptide-like proteins (NLP), and the FMRFamide-related peptides (FLP) (48). We have shown that the *flp* genes are coordinately up-regulated during dauer-commitment. On

the other hand, few of the *ins* genes, and approximately half of the *nlp* genes are up-regulated during dauer-commitment. The low level of *ins* up-regulation is not surprising since insulins have conserved roles in growth and metabolism in Metazoa (80). In addition, signaling through the *C. elegans* insulin-like receptor DAF-2 promotes reproductive growth (48). Indeed, the only *ins* gene that was up-regulated between dauer-commitment and L4 was *ins-1*, which is known to increase dauer entry, likely by antagonizing DAF-2 signaling (28). Likewise, the *nlp* genes would not be expected to be up-regulated as a family either, since the NLPs are a miscellaneous group of non-INS, non-FLP neuropeptides (48) that likely function in several independent processes. On the other hand, FLPs have conserved roles in regulating feeding and reproduction in nematodes, arthropods, mollusks, and vertebrates (80-83). These roles correlate well with the inhibition of feeding and reproduction, and the activation of specialized food-seeking behaviors in dauer. Therefore, the coordinated up-regulation of the *flp* family may function to generate a wide response to stress that is centered on feeding and reproduction control.

We took advantage of the knockdown of neuropeptide processing in *sbt-1(ok901)* null mutants (26) to investigate the function of the neuropeptides during dauer development. We have shown that the net effect of peptidergic signaling downstream of *sbt-1* is to promote dauer entry, perhaps by encoding pro-dauer information from the sensed environment, or by modulating the food, temperature, and pheromone signaling pathways to affect the threshold (13) for dauer entry. We have also assayed 23 *flp* mutants and observed increased dauer entry in 4 mutants and decreased entry in 8 mutants. These results suggest that FLPs can act redundantly and with opposed effects on dauer entry, perhaps to fine-tune the entry decision in response to environmental signals.

Following dauer entry, dauer larvae demonstrate behaviors and preferences that are not observed in non-dauers. For instance, dauers are the only stage that can nictate (10, 19), and are attracted to CO_2 while non-dauers are repelled (18, 84). These changes indicate that dauers possess a different neural state from non-dauers, likely involving different or altered circuits in the nervous system. Yet, *C. elegans* possesses only 302 neurons that are densely interconnected (79, 85), with no synaptically compartmentalized circuits to switch between during dauer and non-dauer. To overcome this constraint, dauers can rewire their neurons to access new behaviors (16, 19). We observed that in addition to this strategy, peptidergic signaling downstream of *sbt-1* promotes coordination during nictation, and is necessary for the switch from CO_2 repulsion to CO_2 attraction in dauer. We have also shown that the combined effects of *flp-10* and *flp-17* strongly promote nictation coordination and the switch to CO_2 attraction. Therefore, we have demonstrated that neuropeptides change the neural state of *C. elegans* during dauer, possibly by altering the composition and function of the active circuits in the nervous system (**Figure 2.12**).

Considering these results, it is notable how many neuropeptides are up-regulated during dauer development. By dauer, 64 neuropeptide genes encoding 215 peptides are up-regulated, and by comparison, the entire human genome only contains 97 neuropeptide genes encoding 270 peptides (56). Indeed, the neuropeptide gene families are expanded in *C. elegans* (48), and the FLP neuropeptides are especially expanded in the phylum Nematoda (27). We observed that FLPs are involved in establishing the *C. elegans* dauer neural state, and RNAi knockdown experiments have also shown that FLPs regulate the IJ dispersal behaviors of *G. pallida* (*flp-12*), *Meloidogyne incognita* (*flp-18*), and *Steinernema carpocapsae* (*flp-21*) (86, 87), indicating that they are involved in establishing the IJ neural

state as well. Because we observed coordinated up-regulation of the FLPs during dauer, and in the IJs of the distantly related nematodes *S. stercoralis*, *A. ceylanicum*, and *G. pallida*, we speculate that the computational challenges of dauer and IJ were the driving force for *flp* expansion in Nematoda. This hypothesis is supported by the lack of such expansion in the nematodes *Trichinella spiralis* and *Trichuris muris* (69), which do not posses dauer or IJ stages (88, 89), and only encode 4 *flp* genes each. Therefore, *flp* expansion may have provided ancestral nematodes the means to overcome their constrained nervous systems (90) in order to effectively adapt to stress during dauer and IJ.

Our genetic data and meta-analysis also suggest that SBT-1 would be a potent target for anthelminthic control. Since *sbt-1* nulls are strongly defective in dauer entry and dispersal behaviors, we predict that targeting SBT-1 in parasitic nematodes will severely impair dispersal and host-seeking in their IJs. While RNAi against individual FLPs can affect IJ dispersal (86, 87), our meta-analysis indicates that multiple FLPs are up-regulated in several types of parasitic nematodes. We propose that inhibition of SBT-1 could be used to efficiently knock down multiple FLPs at once, and in a wide range of parasitic nematodes. SBT-1 would also be an excellent target, since nematode SBT-1 is distinct in sequence from vertebrate 7B2 (57), reducing the risks of cross-species effects.

Altogether, we have investigated phenotypic plasticity in a whole organism by studying *C. elegans* adaptation to stress during development. We uncovered the transcriptional dynamics of *C. elegans* during dauer development, and discovered a strategy of massively up-regulating neuropeptide expression. This strategy functions to enhance the dauer entry decision and expand the behavioral repertoire of dauers, and appears to be evolutionarily shared by dauers and host-seeking IJs, suggesting SBT-1 as a potent anthelminthic target.

2.5 Materials and Methods

Animal strains

C. elegans strains were grown using standard protocols with the *E. coli* strain OP50 (for plate cultures) or HB101 (for liquid cultures) as a food source (91). The wild type strain was N2 (Bristol). PS5511 *daf-9(dh6)*; *dhEx24* was a gift from the Antebi lab. Strains obtained from the *Caenorhabditis* Genetics Center (CGC) include: NY16 *flp-1(yn4)*, VC2324 *flp-6(ok3056)*, RB1990 *flp-7(ok2625)*, PT501 *flp-8(pk360)*, RB1989 *flp-10(ok2624)*, FX02706 *flp-11(tm2706)*, RB1863 *flp-12(ok2409)*, AX1410 *flp-18(db99)*, RB2188 *flp-20(ok2964)*, RB982 *flp-21(ok889)*, VC1982 *flp-25(gk1016)*, and VC3017 *flp-26(gk3015)*. AX1129 *flp-21(pk1601*) was a gift from the De Bono lab. MT15933 *flp-17(n4894)* and MT15973 *flp-10(n4543); flp-17(n4894)* were gifts from the Horvitz lab. PS7112 *sbt-1(ok901)* was outcrossed 6 times from CGC RB987; PS7370 *flp-2(ok3351)* was outcrossed 3 times from CGC VC2591; PS7378 W07E11.1 & *flp-2(gk1039)* was outcrossed 3 times from CGC VC2490; PS7379 *flp-3(ok3265)* was outcrossed 3 times from CGC VC2497; PS6813 *flp-13(tm2427)* was outcrossed 3 times from the Mitani strain FX02427; and PS7221 *flp-34(ok3071)* was outcrossed 3 times from CGC RB2269.

Transgenic strains

sbt-1 genomic DNA rescue strains were generated by injecting 15 ng/µL of *sbt-1* genomic DNA (amplified by PCR with forward primer CTGTGAAGCGCTCATCTGAA and reverse primer TTCAGGCAAATCCATCATCA), 50 ng/µL coelomocyte-specific *ofm-1p::rfp* co-injection marker, and 135 ng/µL 1 kb DNA ladder (New England Biolabs,

Beverly, MA) carrier DNA into the adult gonads of *sbt-1(ok901)* animals, followed by integration into the genome by X-ray (92, 93). Two independent integration lines were generated: PS7274 *sbt-1(ok901); Is444[sbt-1p::sbt-1; ofm-1p::rfp]* (line 1, outcrossed 2 times) and PS7275 *sbt-1(ok901); Is445[sbt-1p::sbt-1; ofm-1p::rfp]* (line 2, outcrossed 3 times).

Transcriptional reporter strains

Transcriptional reporter constructs were built using fusion PCR (1). The promoter regions of *srt-41* and *col-40* were fused to *mCherry*::*unc-54* 3'UTR (amplified from pGH8 from Addgene). The flanking sequences of the amplified *srt-41* promoter were GCACAGTTTTAAGTTTTTCTGTCTT and TGCTGCCAACCTGTTCTG. The flanking sequences of the amplified *col-40* promoter were ATGATGACCGCCTGATTTTC and AATTATTGTAGTAAAGGGGGAAGTC. Injection mixtures were prepared at a concentration of 20 ng/µL reporter construct, 50 ng/µL *unc-119(+)* rescue construct, and 130 ng/µL 1 kb DNA ladder carrier DNA. Transgenic animals were obtained by microinjecting the mixtures into the adult gonads of *unc-119(ed4)* animals (2, 3). The fluorescent transcriptional reporter strains that were generated are:

PS7128 *unc-119(ed4); syEx1534[srt-41p::mCherry; unc-119(+)]* and

PS6727 *unc-119(ed4); syEx1338[col-40p::mcherry; unc-119(+)]*

CRISPR-generated strains

CRISPR mutagenesis with co-conversion (94) was used to generate the deletion strains. Guide RNA (gRNA) target sequences of 19 bp (corresponding to sequence upstream of an

NGG PAM site) were cloned into pRB1017 single-guide RNA (sgRNA) vector (Addgene). Four distinct gRNA sequences were used to target each gene. Injection mixtures were prepared at a concentration of 25 ng/µL per sgRNA expression plasmid, 50 ng/µl Cas9 plasmid (Addgene #46168), 25 ng/µl *dpy-10* sgRNA plasmid (pJA58 from Addgene), and 500 mM *dpy-10(cn64)* donor oligonucleotide (synthesized by Integrated DNA Technologies, Coralville, IA). Injected P_0 hermaphrodites were transferred to individual Petri plates to produce F_1 progeny. F_1 progeny exhibiting a Rol or Dpy phenotype were picked to individual Petri plates four days after injection. F_1s that produced Rol or Dpy F_2s were genotyped for the presence of a deletion allele. Homozygous deletion mutants were isolated from the F_2 or F_3 population, and the deletion alleles were confirmed by Sanger sequencing (Laragen, Culver City, CA).

The 1343bp *flp-21(sy880)* deletion is flanked by the sequences TATGTACACTATTTAA GATTTGATTGTGTA and CATTCGGGGCCACAAACTCCTGCTTCGATC. *flp-32(sy853)*, *flp-34(sy810)* and *flp-34(sy811)* deletion alleles have short DNA fragment insertions. The 460bp *flp-32(sy853)* deletion is flanked by the sequences TATGAATATGTTCCGGAGCGCATGTCAAAC and AACTAAAGATACACCACTAC CACCTGAACC, with a TAACT insertion. The 1365bp *flp-34(sy810)* deletion is flanked by the sequences TCAAATTTTTTGAGGAAATCCTCCTGAAAC and AATATTTTCGA GTTTCGAAACATTTCAAAT, with a AATATATTTTCGAGTTTCGAAACATATTTT CGAGTTTCGAAACAC insertion. The 1607bp *flp-34(sy811)* deletion is flanked by the sequences TTTGTGTCTAGCAAAAGGAGATGCTCTTTA and CATAGGCGTAGGCC ATAGGCGTAGGCCATA, with a AATAAATTAATTAAATATCTGAAATAAAAACA

AAACCTCGAGAGAGAAAATTTAGAAAAAAAAACGAGACGGCTACGGACGGCT
GACGTGATGGAATTATTTACGGCCAAATCTGAAAATAAAATGGATTATATTTT
GTTTTAGGCCATAGACGTAGGTCATAGGCGTAGACCATAGGCGTAGGC
insertion.

***daf-9(dh6)* culturing and harvesting for RNA-seq**

Synchronous, single-stage populations of *daf-9(dh6)* animals were grown using our previously described method for liquid culturing *daf-9(dh6)* (13). *daf-9(dh6)* animals were collected at 6 points over a branching time series along 24 hours post hatch (hph) to 60 hph. This period, as we have previously analyzed, includes L2d sensory integration, dauer-commitment, dauer maintenance, reproductive-commitment, and reproductive development (13) (**Figure 2.1A**). The dauer-developing branch was obtained by withholding dafachronic acid (Δ7-DA), and animals were collected at 24 hph (L2d), 26 hph (L2d), 34 hph (dauer-commitment), and 60 hph (dauer). The reproductive-developing branch was obtained by adding 100 nM Δ7-DA at 24 hph, and animals were collected at 26 hph (L3-committing) and 34 hph (L4). Reproductive animals at 60 hph are gravid, making them inappropriate for single-stage transcriptome analysis, and were therefore not collected.

Cultures from the dauer and reproductive branches were grown in parallel, fed at the same time, and experienced the same batches of HB101 and Δ7-DA in order to minimize asynchronous development between the cultures. Each time point was collected using two independently cultured biological replicates. Each biological replicate was maintained separately for at least 5 generations. Harvested animals were spun in S. Basal three times to

help clear the bacteria. The worm pellets (approximately 10,000 worms per pellet) were then treated with 1 mL Trizol and 0.6 mg/mL linear polyacrylamide carrier, before being flash frozen in liquid nitrogen and stored at -80°C. RNA was purified as previously described (13).

RNA-sequencing and computational analysis

cDNA was prepared from the collected samples using the Illumina TruSeq RNA Sample Preparation kit or mRNA-Seq Sample Preparation kit. cDNA was sequenced using the Illumina HiSeq2000 to generate paired-end or single-end libraries. Paired-end libraries were not multiplexed, were sequenced at a read length of 100 bp, and were sequenced to an average depth of 76 million reads. Single-end libraries were multiplexed at 4 libraries per lane, sequenced at a read length of 50 bp, and sequenced to an average depth of 33 million reads. All raw sequences have been deposited into the NCBI Sequence Read Archive (SRA) database (accession number SRP116980). **Appendix Table 2.1** contains the detailed metadata for the sequenced libraries. Codes used for data analysis have been deposited into GitHub at https://github.com/WormLabCaltech/dauerRNAseq.

***Read mapping and differential expression testing*:** Reads that did not pass the Illumina chastity filter were removed using Perl. Read mapping, feature counting, library normalization, quality checks, and differential gene expression analysis was performed using R version 3.1.0, bowtie2 version 2.2.3, tophat2 version 2.0.12, SAMtools version 0.1.19, HTSeq version 0.6.1, and DESeq, as described in (38). The *C. elegans* reference genome and gene transfer format files were downloaded from Ensembl release 75 and genome assembly WBcel235. Gene dispersion estimates were obtained after pooling all

sequenced samples. Each pairwise comparison for differential gene expression was performed at a Benjamini-Hochberg controlled false discovery rate < 0.01.

***RNA-seq data summaries*:** Principal component analysis was performed using the DESeq package in R (37). Violin plotting was done in R using ggplot2 (95). KEGG biochemical pathway enrichment analysis was performed using clusterProfiler in R (96), at a cutoff of BH-corrected *q*-value < 0.01. Gene Ontology (GO) enrichment analysis was performed using the PANTHER Overrepresentation Test for GO Biological Process, at a Bonferroni-adjusted *p*-value cutoff of < 0.05. GO and KEGG terms were ranked based on descending fold-enrichment for GO, and ascending *q*-value for KEGG.

***Soft clustering*:** Soft clustering was performed using the mFuzz package in R (40, 41). Gene expression data were standardized before clustering, and cluster numbers were chosen based on cluster stability, minimum cluster centroid distance, and visual clarity of the clusters. Over-represented neuronal gene classes in clusters 1 to 6 were determined by hypergeometric test, using a cutoff of Bonferroni-corrected *p*-value < 0.05.

***Heatmaps*:** Heatmaps were drawn using the gplots and RColorBrewer packages in R (97, 98). Mean count values were used for each time point, calculated by averaging the biological replicates. Heatmap dendrograms were drawn using correlation distances and average-linkage hierarchical clustering. Expression values were centered and scaled for each gene.

***Gene expression correlation analysis*:** Spearman correlation scores were computed using Python 2.7.9 and the Scipy library (99) by ranking the transcripts per million (TPM) values in each RNA-seq experiment, then calculating the Pearson correlation on the ranked values for each pairwise combination of genes: ρ = covariance(gene1, gene2) /σ_{gene1} σ_{gene2}, where

σ represents standard deviation. *p*-values were computed by comparing average correlation scores to the bootstrap distribution of average scores for random sets of 31 genes (mimicking the size of the *flp* family), and calculated as the fraction of times that bootstrapping produced a score greater than or equal to the score being tested. Because the *ins* and *nlp* families have more than 31 genes, the *p*-value is an upper estimate. Bootstrapping was performed 10,000 times. The RNA-seq datasets that were used were our *daf-9(dh6)* RNA-seq data, re-quantified using kallisto (100) into TPM counts; and processed RNA-seq data from 246 publically available libraries (23), obtained using WormBase SPELL and converted to TPM counts (101). Genes detected in less than 80% of the experiments were discarded.

***Dotplot analysis*:** Dotplot analysis of the *flp* coding sequences was performed using Gepard (63). Coding sequences from the 31 total *flp* genes (taking only the a isoform for genes with multiple isoforms) were used in the analysis.

Dauer entry assay on pheromone plates

The preparation of crude pheromone and the dauer entry assay were performed with modifications to previously described methods (102). Crude pheromone was extracted from exhausted liquid culture medium, re-suspended with distilled water and stored at -20°C. Pheromone plates (NGM-agar with added crude pheromone and no peptone) were freshly prepared the day before each experiment and dried overnight at room temperature. Heat-killed *E. coli* OP50 was used as a limited food source for the dauer entry assays, and was prepared by re-suspending OP50 overnight cultures in S. Basal to 8 g/100 mL, and heating at 100°C for 5 minutes. On the day of the experiment, seven to ten

young adults were picked onto each plate, and allowed to lay approximately 50-60 eggs before being removed. 20 μl of heat-killed OP50 was added to the plates as a food source for the un-hatched larvae. After 48 hours of incubation at 25.5°C, dauers and non-dauers were counted on each plate based on their distinct morphologies.

Dauer entry can exhibit day-to-day variation caused by environmental conditions such as humidity or temperature (25). To control for this variation, wild type controls were run in every trial. The wild type results from the same batch of pheromone were pulled together for better statistical power, and each statistical analysis was done with samples treated with the same batch of pheromone.

Statistical analysis for dauer entry assay

The mean and 99% confidence interval of the dauer entry percentage were calculated non-parametrically for each genotype by pooling the data from all the plates and computing 10,000 bootstrap replicates (103). Pairwise comparisons were performed through a non-parametric permutation test with 10,000 replicates. The difference in dauer entry probability between two genotypes was estimated using a Bayesian approach (104) to compute the posterior probability of dauer entry for each genotype. Bootstrapping, permutation, and Bayesian statistics were performed using Python 3.5 and the SciPy library (105).

For each genotype, the data from all of the plates tested for that genotype were pooled and the number of dauers and non-dauers were converted into a Boolean array (1 for dauer, 0

for non-dauer). Non-parametric bootstrapping was used to sample the data array (with replacement) to calculate a corresponding dauer entry percentage. This procedure was repeated 10,000 times to construct a dauer entry percentage distribution, from which the mean and 99% confidence interval were calculated.

For each comparison between two genotypes, data arrays from the two genotypes were concatenated, shuffled, and split into two datasets of original size as before concatenation, and a difference of means was calculated between the two new datasets. This procedure was repeated 10,000 times to generate a distribution of differences of means that simulated the null hypothesis. The *p*-value was calculated as the fraction of the distribution where the simulated difference was greater than or equal to the observed difference.

A binomial likelihood was used with a uniform prior for values in the range [0, 1], so that the log posterior probability distribution was proportional to the log bionomial distribution in the allowed range. The data for each genotype were pooled, and the posterior distribution was sampled using Markov chain Montecarlo (MCMC). The difference between mutant and wild-type was computed by subtracting the respective MCMC samples.

Dauer behavior assays

Crude pheromone plates were used to induce synchronized dauers for behavior assays: for each pheromone plate, 20 μL of heat-killed OP50 (8 g/100 mL) were spotted and 12-15 young adult animals were picked onto the plate to lay eggs at 20°C for 12 hours before being removed. After 2-4 days of incubation at 25.5°C, dauers were identified by their morphology and isolated for the following assays.

***Nictation assay*:** Nictaiton assay was performed on micro-dirt chips with modifications to previously described methods (19). Dauers suspended in distilled water were transferred onto the micro-dirt chip (4% agarose in distilled water) and allowed to nictate. Each nictating dauer was observed for at least 3 minutes or until the end of nictation. The time recording began when a dauer initiated nictation (by lifting its neck region of the body), and the total duration of each nictation event was also recorded. If the dauer stopped nictating and exhibited quiescence in a standing posture during the recording, the data were excluded from further analysis. The average nictation duration was calculated by dividing the total duration of nictation by the number of nictation events. At least 20 dauers were assayed for each genotype. The mean of average duration and 99% confidence interval, and the pairwise *p*-value, were computed non-parametrically as described for the dauer entry assay.

***CO_2 chemotaxis assay*:** CO_2 chemotaxis assays were performed on dauers with modifications to previously described methods (18). Dauers were washed three times with distilled water and transferred to standard chemotaxis assay plates (106). Two gas mixtures were delivered to the plate at a rate of 0.5 mL/min through PVC tubing and holes drilled through the plate lid. The CO_2 gas mixture was 10% CO_2 and 21% O_2 balanced with N_2, and the control gas mixture was 21% O_2 balanced with N_2 (Airgas). The two holes were positioned on opposite sides of the plate along a diameter line, with each of them positioned 1 cm from the edge of the plate. The scoring regions were set as the areas of the plate beyond 1 cm from a central line drown orthogonally to the diameter on which the gas mixtures were presented. At the end of 1 hour, the numbers of animals in each scoring region was counted and the chemotaxis index was calculated as ($N_{at\,CO2}$ scoring region $- N_{at}$

$_{\text{control gas}}$ scoring region) / ($N_{\text{at CO2}}$ scoring region + $N_{\text{at control gas}}$ scoring region). Statistical analysis (two-tailed t test) was performed using GraphPad Prism.

***Acute CO_2 avoidance assay*:** CO_2 avoidance assays were performed as previously described (62), with slight modifications. Dauers were washed three times with distilled water and transferred to unseeded NGM plates. A 50 mL gas-tight syringe was filled with either a CO_2 gas mixture or a control gas mixture, and connected to a pipet tip using PVC tubing. Gas was pumped out through the pipet tip at a rate of 1.5 mL/min using a syringe pump, and the tip was presented to the head of forward-moving dauers. A response was scored if the animal reversed within 4 seconds. For each plate, at least 20 animals were assayed per gas mixture, with each plate counted as a trial. The avoidance index was calculated as ($N_{\text{reversed to CO2}}$ / $N_{\text{presented with CO2}}$) − ($N_{\text{reversed to control gas}}$ / $N_{\text{presented with control gas}}$). Statistical analysis (one-way ANOVA with Bonferroni post-correction test) was performed using GraphPad Prism.

flp gene expression in infective juveniles

Orthologs/analogs of *C. elegans flp* genes exist in other nematodes (69, 80, 107). Identified *flp* orthologs/analogs in (69, 107) were matched to transcript IDs in *S. stercoralis*, *A. ceylanicum*, *G. pallida*, and *B. malayi* using BLAST via WormBase ParaSite. Published RNA-seq data was downloaded for *S. stercoralis* (73) and *G. pallida* (71) using the ENA; *B. malayi* (70) using WormBase SPELL; and *A. ceylanicum* (72) as it was published.

The read counts from the *A. ceylanicum* and *B. malayi* data were pre-processed into TPM counts. We obtained TPM counts for the *S. stercoralis* and *G. pallida* datasets using

kallisto to align the read data and to quantify transcript abundances (100). Kallisto was preferable to DESeq at this stage of our analysis, as it allowed us to quickly and accurately quantify these large datasets. To increase comparability between all of the datasets, kallisto was used to re-quantify our own dauer RNA-seq data into TPM counts.

2.6 Figures

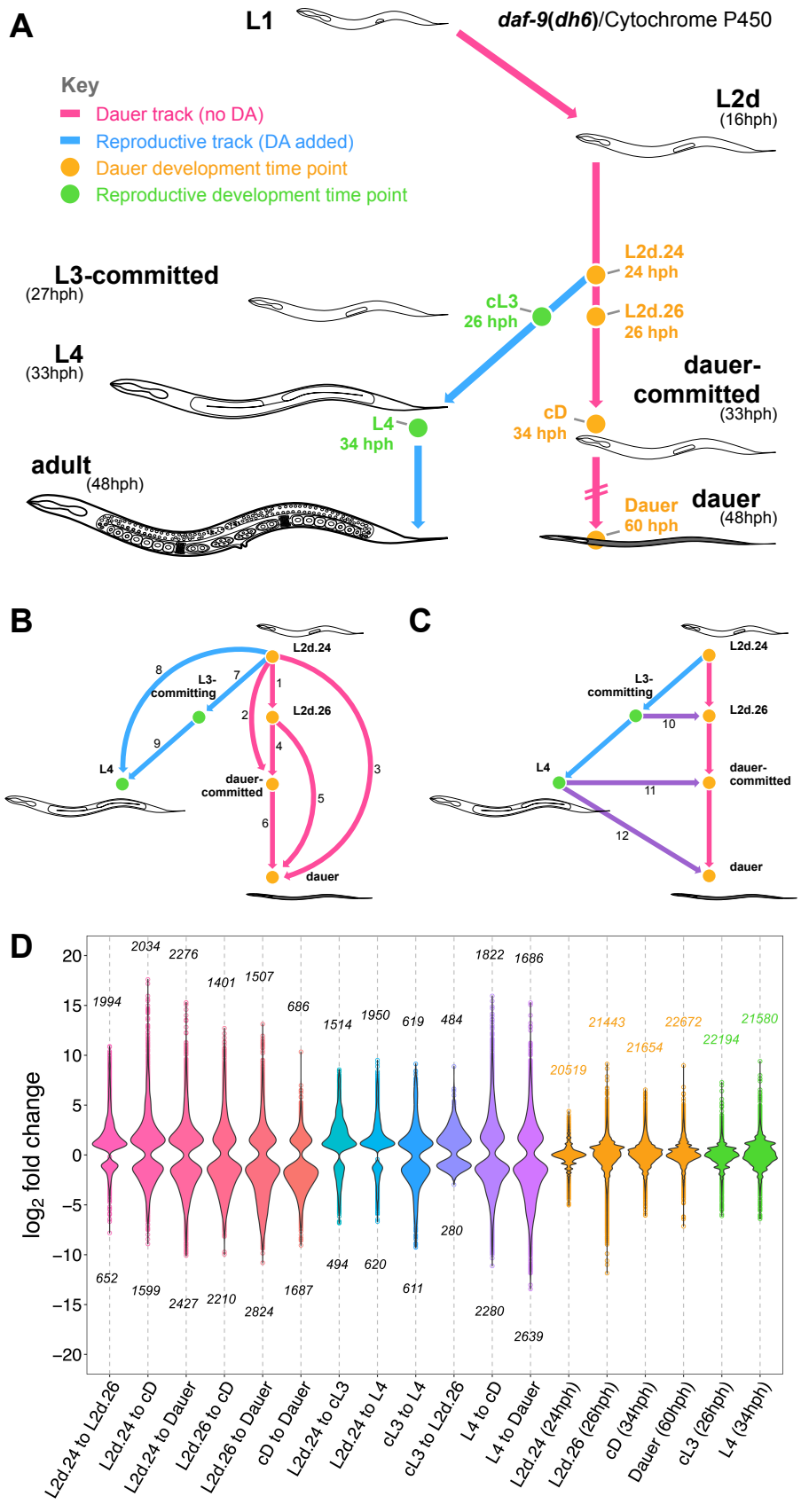
A
L1
daf-9(dh6)/Cytochrome P450
Key
Dauer track (no DA)
Reproductive track (DA added)
Dauer development time point
Reproductive development time point
L2d
(16hph)
L2d.24
24 hph
L3-committed
(27hph)
cL3
26 hph
L2d.26
26 hph
L4
(33hph)
dauer-
committed
(33hph)
cD
34 hph
L4
34 hph
adult
(48hph)
Dauer
60 hph
dauer
(48hph)
B
L2d.24
L3-
committing
L2d.26
L4
dauer-
committed
dauer
C
L2d.24
L3-
committing
L2d.26
L4
dauer-
committed
dauer
D
log2 fold change
20
15
10
5
0
−5
−10
−15
−20
1994
2034
2276
1401
1507
686
1514
1950
619
484
1822
1686
20519
21443
21654
22672
22194
21580
652
1599
2427
2210
2824
1687
494
620
611
280
2280
2639
L2d.24 to L2d.26
L2d.24 to cD
L2d.24 to Dauer
L2d.26 to cD
L2d.26 to Dauer
cD to Dauer
L2d.24 to cL3
L2d.24 to L4
cL3 to L4
cL3 to L2d.26
L4 to cD
L4 to Dauer
L2d.24 (24hph)
L2d.26 (26hph)
cD (34hph)
Dauer (60hph)
cL3 (26hph)
L4 (34hph)

Figure 2.1. 39% of the *C. elegans* genome is differentially expressed during dauer and reproductive development. (A) Experimental design for collecting dauer- and reproductively-developing *daf-9(dh6)* animals. The timing of molt events are indicated in parentheses (13). **(B-C)** Twelve comparisons between the six time points. Arrows are directed from the reference point to the end point of each comparison. **(D)** Violin plots of the significantly up- and down-regulated genes in each comparison. The number of up- and down-regulated genes in each comparison is indicated above and below its violin plot. The fold changes between the replicates of each sequenced time point are plotted for reference (orange and green plots). Abbreviations are hph: hours post hatch, DA: dafachronic acid, cL3: L3-committing, cD: dauer-committed.

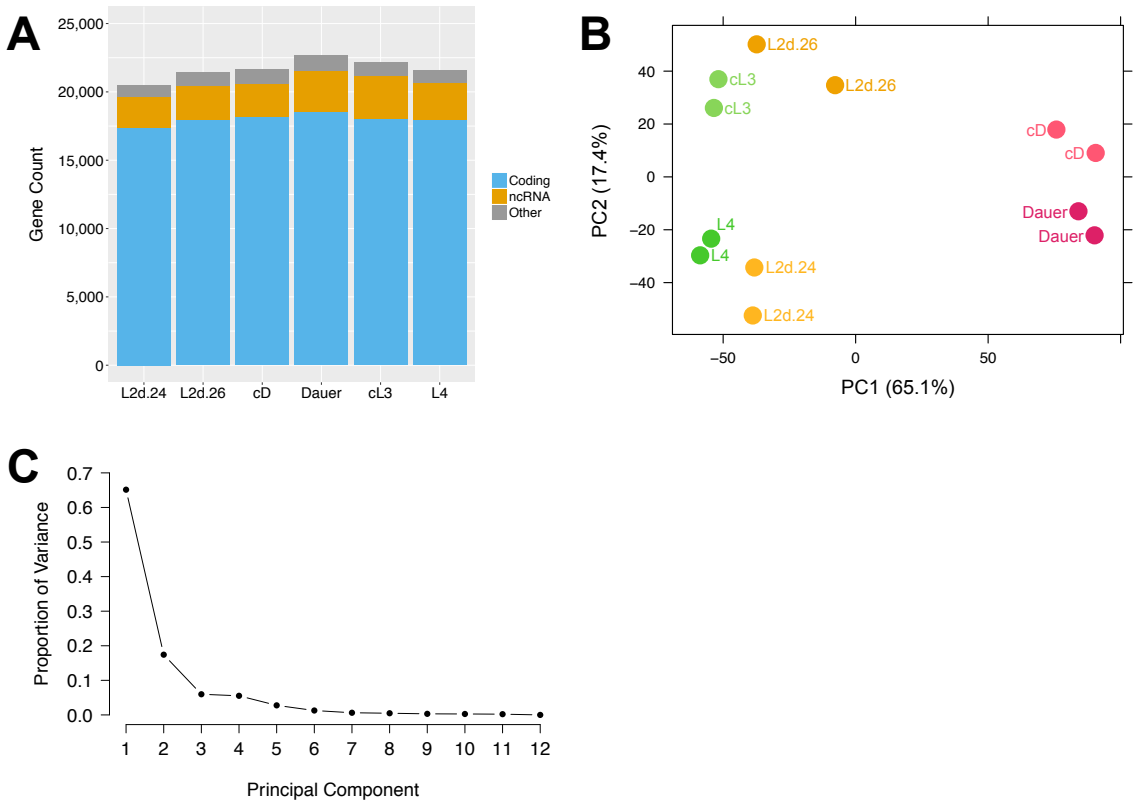

Figure 2.2. ***daf-9(dh6)*** **RNA-seq dataset summaries (A)** Detected gene counts from the six sequenced stages along dauer and reproductive development. **(B)** Principal component analysis plot of the variation in gene expression across the 12 sequenced samples. The proportion of total variation that is spanned by PC 1 and 2 are listed in parentheses. **(C)** Scree plot demonstrating the proportion of the total variation between the 12 sequenced samples that is explained by each principal component in the principal component analysis.

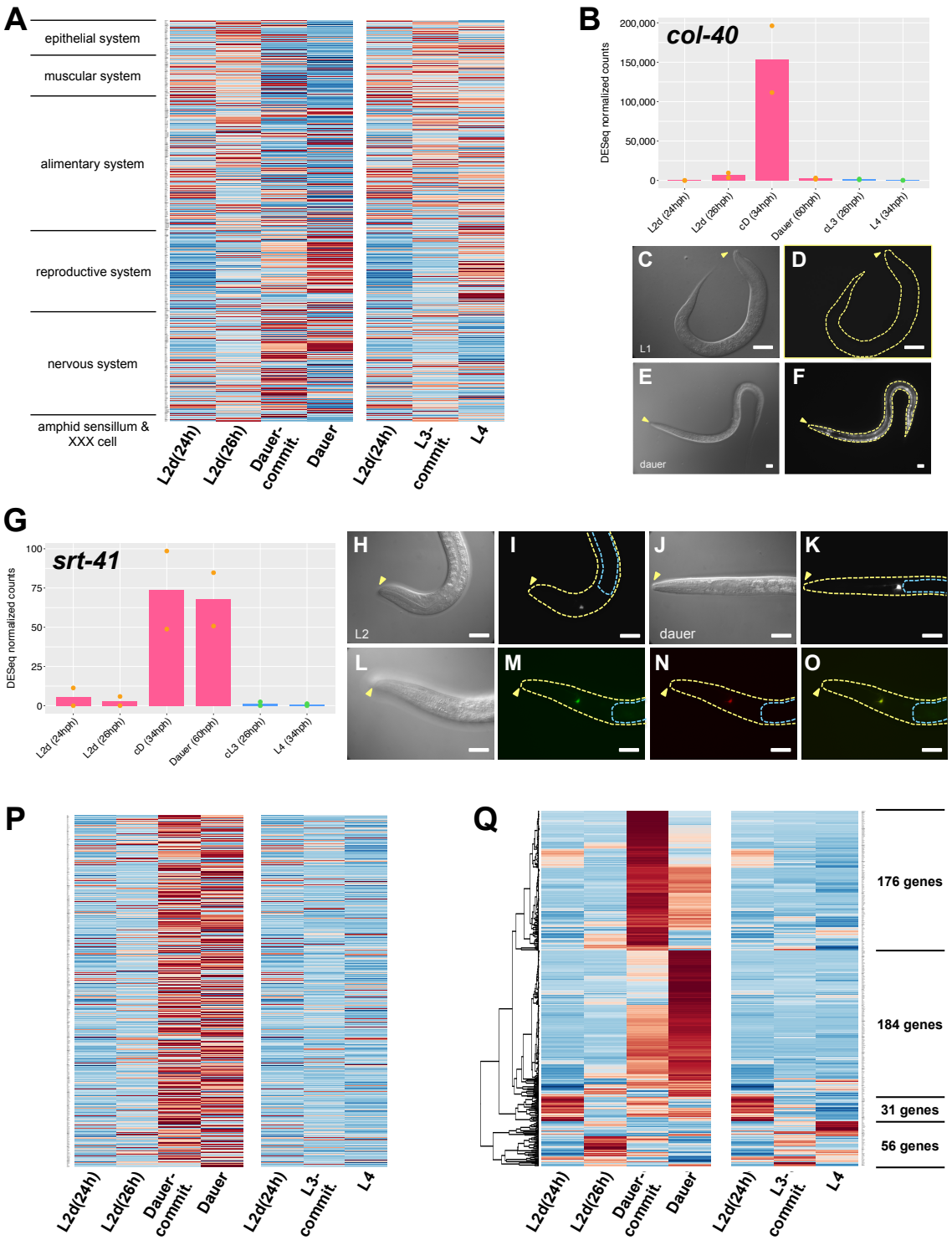
A
epithelial system
muscular system
alimentary system
reproductive system
nervous system
amphid sensillum & XXX cell
L2d(24h)
L2d(26h)
Dauer-commit.
Dauer
L2d(24h)
L3-commit.
L4
B
col-40
DESeq normalized counts
200,000
150,000
100,000
50,000
0
L2d (24hph)
L2d (26hph)
cD (34hph)
Dauer (60hph)
cL3 (28hph)
L4 (34hph)
C
L1
D
E
dauer
F
G
srt-41
DESeq normalized counts
100
75
50
25
0
L2d (24hph)
L2d (26hph)
cD (34hph)
Dauer (60hph)
cL3 (26hph)
L4 (34hph)
H
L2
I
J
dauer
K
L
M
N
O
P
L2d(24h)
L2d(26h)
Dauer-commit.
Dauer
L2d(24h)
L3-commit.
L4
Q
176 genes
184 genes
31 genes
56 genes
L2d(24h)
L2d(26h)
Dauer-commit.
Dauer
L2d(24h)
L3-commit.
L4

Figure 2.3. Differential expression was detected at high accuracy and single-cell resolution (A) The expression profiles of differentially expressed genes with putative tissue-specific expression in the epithelial system, muscular system, alimentary system, reproductive system, nervous system, amphid sensillum, and XXX cell. The expression data was scaled and heatmapped as in Figure 3. (B) Detected read counts for the col-40 gene. Points indicate count values from each sequenced replicate. The bar height represents the mean count value for each stage. Abbreviations are hph: hours post hatch, cL3: L3-committing, cD: dauer-committed. (C-D) Bright field and fluorescence images of the col-40 non-dauer expression pattern (shown is an L1). The body is traced in yellow dotted lines, and yellow arrows point to the mouth for reference. Scale bars represent a length of 20 μm. (E-F) Bright field and fluorescence images of the *col-40* dauer expression pattern. (H-I) Bright field and fluorescence images of the *srt-41* non-dauer expression pattern (shown is an L2). The intestine is traced in blue dotted lines for reference. (J-K) Bright field and fluorescence images of the *srt-41* dauer expression pattern. The two fluorescence images (I) and (K) were captured using the same imaging parameters. (L-O) *srt-41p::mCherry* expression in the AWC^{on} neuron. (M) GFP expressed from the AWC^{on} marker *str-2p::gfp* and (N) mCherry from *srt-41p::mCherry* co-localized in the same cell, as shown in (O) the merged image. Pictured is a non-dauer, since *str-2p::gfp* changes expression to the ASI neuron in dauers (4). (P) Venn diagram comparing our dataset to SAGE data published by Jones, et al. (2001), and microarray data published by Wang & Kim (2003), drawn using the eulerr package (5). Differential expression in our data was tested for using comparisons 2-6 and 11-12 to identify genes that were significantly up-regulated at dauer-commitment and dauer, relative to L2d and L4.

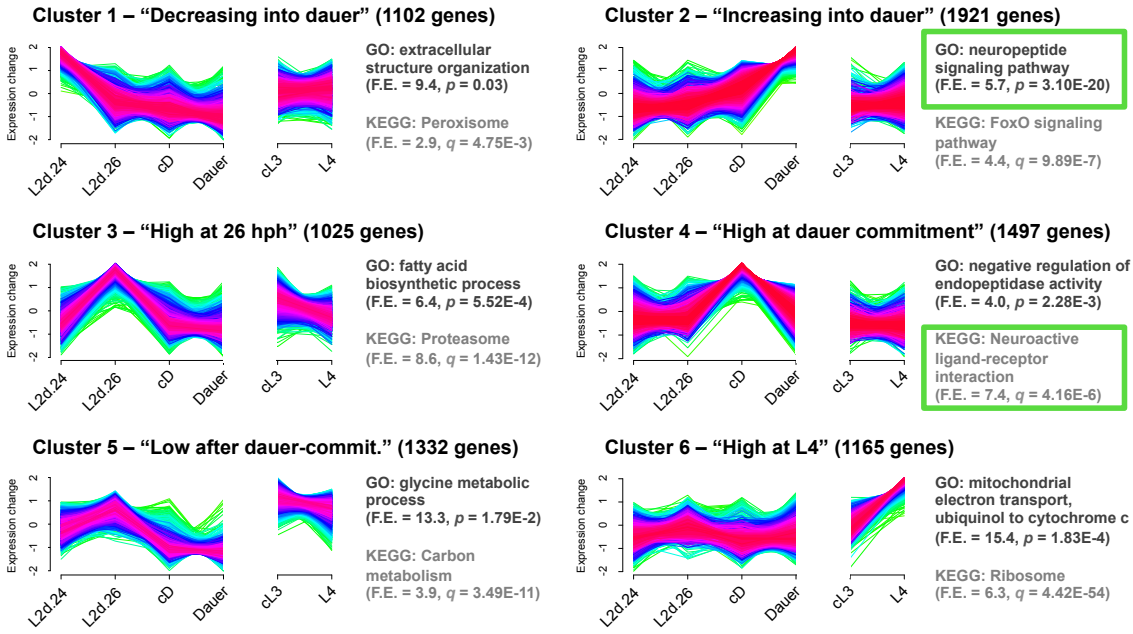

Figure 2.4. Clustering revealed six common expression profiles during dauer and reproductive development.

Soft clustering of the 8,042 differentially expressed genes into six common expression profiles. Yellow-green lines indicate genes with low cluster membership scores, and purple-red lines indicate genes with high membership scores. The top enriched GO and KEGG terms for each cluster are listed. Abbreviations: FE: fold enrichment.

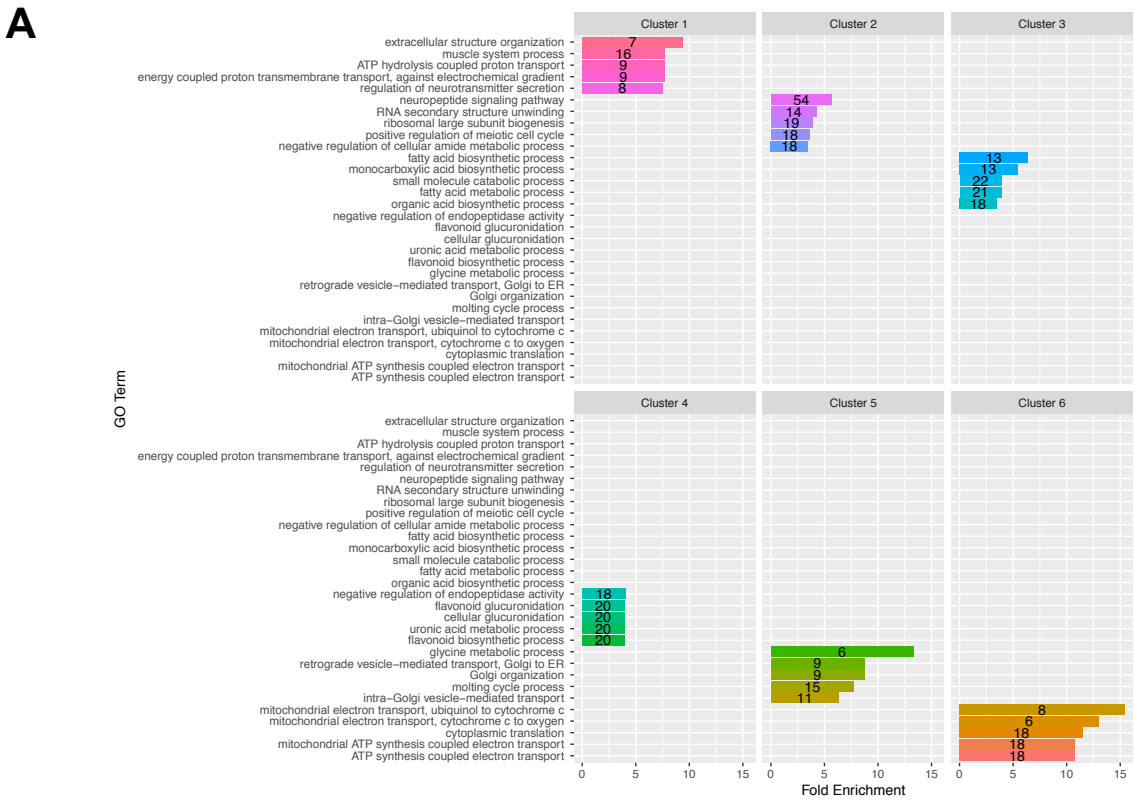
A
Cluster 1
Cluster 2
Cluster 3
Cluster 4
Cluster 5
Cluster 6
GO Term
extracellular structure organization
muscle system process
ATP hydrolysis coupled proton transport
energy coupled proton transmembrane transport, against electrochemical gradient
regulation of neurotransmitter secretion
neuropeptide signaling pathway
RNA secondary structure unwinding
ribosomal large subunit biogenesis
positive regulation of meiotic cell cycle
negative regulation of cellular amide metabolic process
fatty acid biosynthetic process
monocarboxylic acid biosynthetic process
small molecule catabolic process
fatty acid metabolic process
organic acid biosynthetic process
negative regulation of endopeptidase activity
flavonoid glucuronidation
cellular glucuronidation
uronic acid metabolic process
flavonoid biosynthetic process
glycine metabolic process
retrograde vesicle−mediated transport, Golgi to ER
Golgi organization
molting cycle process
intra−Golgi vesicle−mediated transport
mitochondrial electron transport, ubiquinol to cytochrome c
mitochondrial electron transport, cytochrome c to oxygen
cytoplasmic translation
mitochondrial ATP synthesis coupled electron transport
ATP synthesis coupled electron transport
0
5
10
15
Fold Enrichment

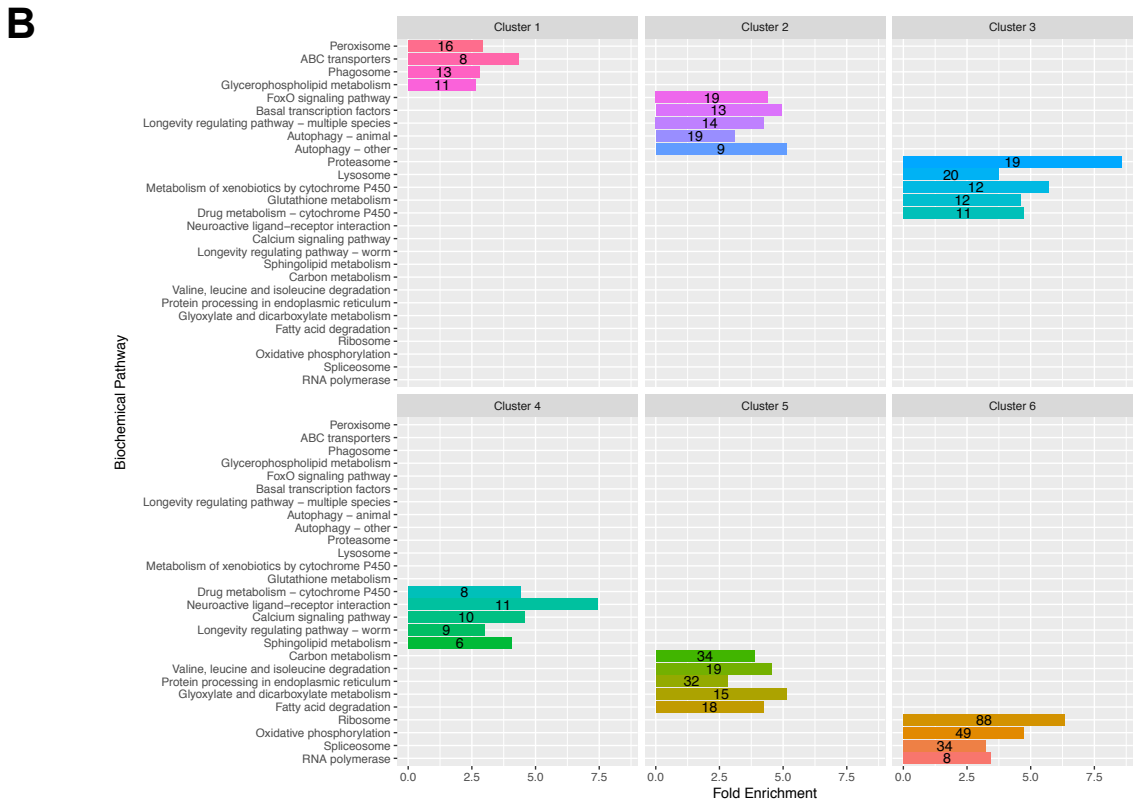
B
Cluster 1
Cluster 2
Cluster 3
Cluster 4
Cluster 5
Cluster 6
Biochemical Pathway
Peroxisome
ABC transporters
Phagosome
Glycerophospholipid metabolism
FoxO signaling pathway
Basal transcription factors
Longevity regulating pathway − multiple species
Autophagy − animal
Autophagy − other
Proteasome
Lysosome
Metabolism of xenobiotics by cytochrome P450
Glutathione metabolism
Drug metabolism − cytochrome P450
Neuroactive ligand−receptor interaction
Calcium signaling pathway
Longevity regulating pathway − worm
Sphingolipid metabolism
Carbon metabolism
Valine, leucine and isoleucine degradation
Protein processing in endoplasmic reticulum
Glyoxylate and dicarboxylate metabolism
Fatty acid degradation
Ribosome
Oxidative phosphorylation
Spliceosome
RNA polymerase
0.0
2.5
5.0
7.5
Fold Enrichment

Figure 2.5. Enriched GO terms and KEGG pathways in clusters 1 to 6. The number in each bar indicates the number of genes with that term in the cluster. (A) The five most enriched GO terms (based on descending fold enrichment) in clusters 1 to 6, using a cutoff of Bonferroni-adjusted p-value < 0.05. (B) The five most enriched biochemical pathways (based on ascending q-value) in clusters 1 to 6, using a cutoff of BH-corrected q-value < 0.05.

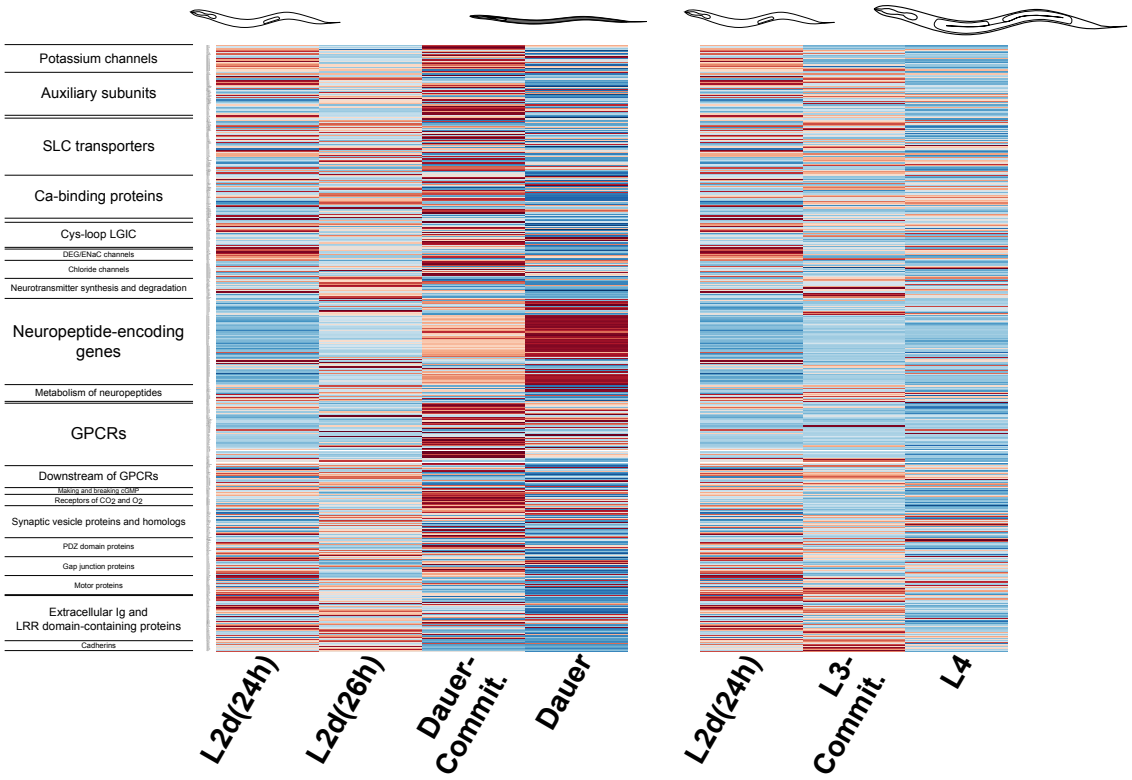

Figure 2.6. Differential expression of the neuronal effector genome of *C. elegans* during dauer and reproductive development. Heatmap of the expression of 606 differentially expressed neuronal effector genes. Each row represents a single gene, with the class that the gene belongs to indicated on the left. Red and blue indicate high and low expression scores, respectively.

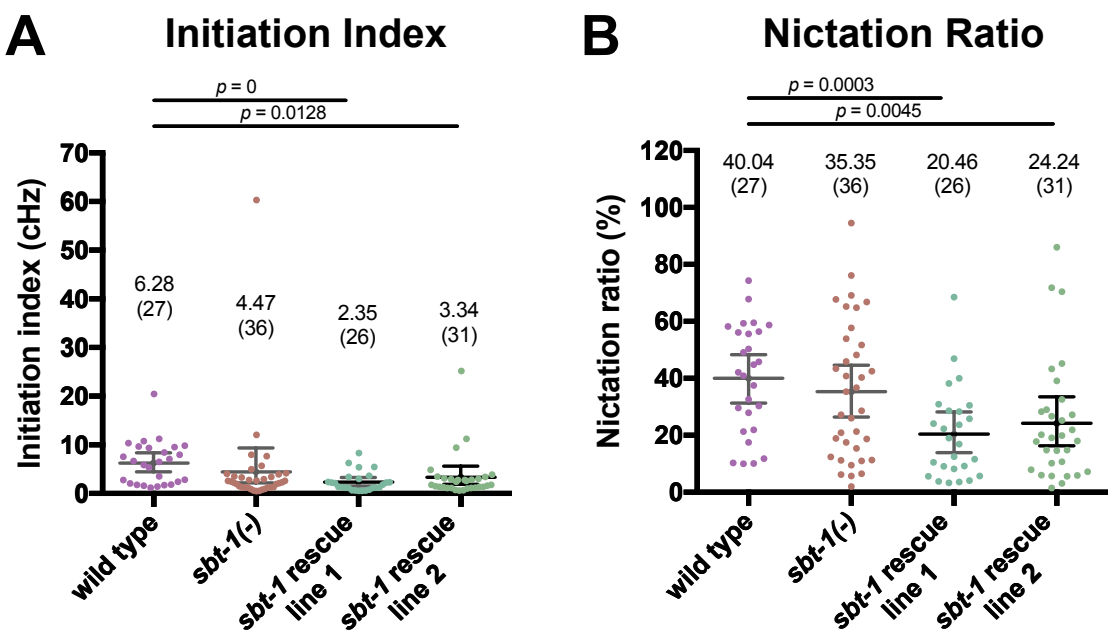

Figure 2.7. Nictation initiation and the proportion of time spent nictating are not significantly affected in *sbt-1* null mutants. (A-B) Nictation initiation (A) and ratio (B) measurements that were collected simultaneously with the nictation duration data in Figure 4D. Bootstrapped means and 99% confidence intervals are indicated. Statistic: permutation test.

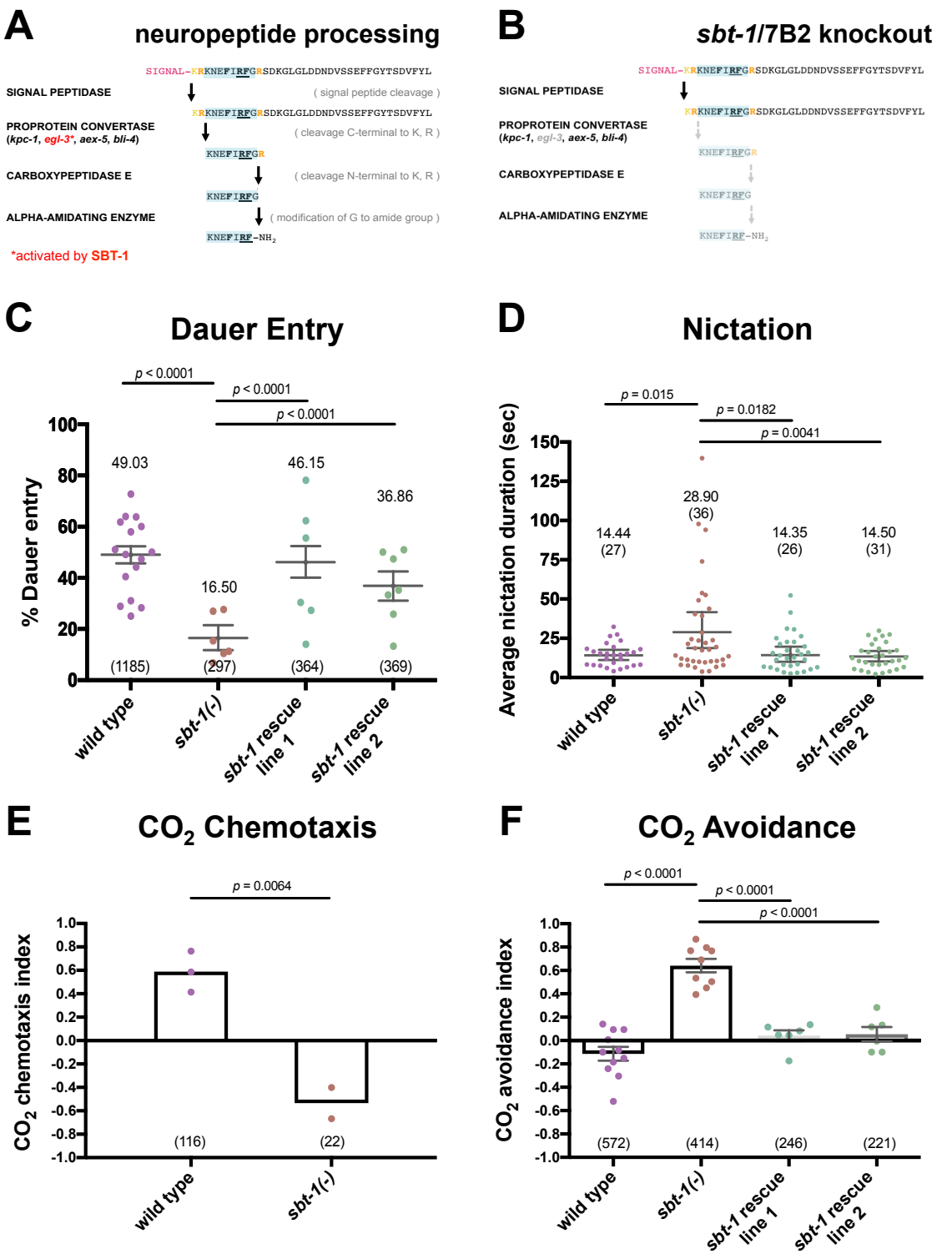

Figure 2.8. Neuropeptide signaling promotes dauer entry and dispersal behaviors. (A-B) Neuropeptide processing in wild type (A) and *sbt-1* null (B), using the FLP-8 peptide

sequence as an example. (C-D) Dauer entry (C) and nictation duration (D) assays. Bootstrapped means and 99% confidence intervals are indicated. (E-F) CO_2 chemotaxis (E) and avoidance (F) assays. Means and SEM are indicated. For (C-F), each dot is one trial, and the N tested is in parentheses. Statistic: permutation test (C-D), two-tailed t (E), one-way ANOVA (F).

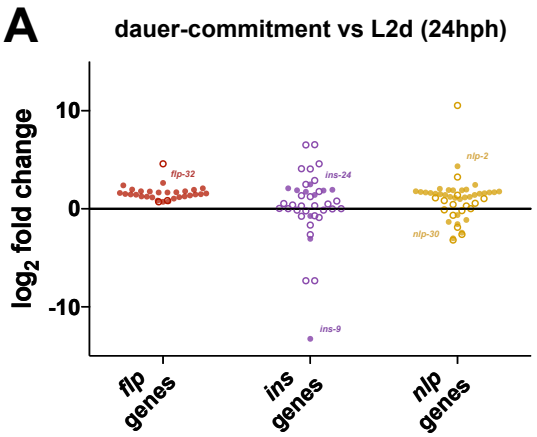

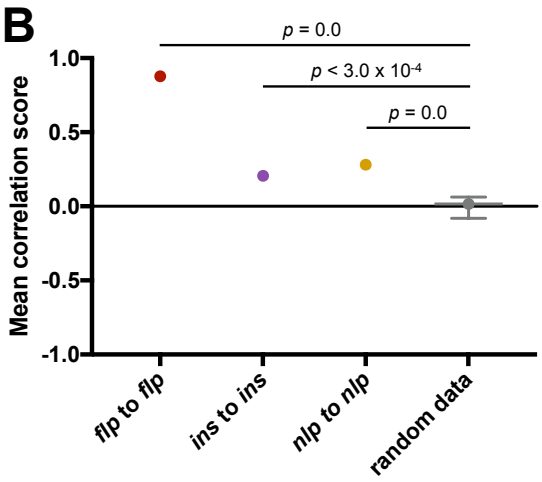

C Dauer Entry

Genotype	Mutant dauer entry %[a]	Wild type dauer entry %[a]	Δ Dauer entry prob.[b]	*p* value[c]	Significance[d]	N mutants tested	N wild type tested	Strain tested
flp-1(yn4)	12.12	72.27	-0.59	0.000	****	99	743	NY16
flp-2(ok3351)	81.15	46.51	0.34	0.000	****	260	744	PS7370[g]
W07E11.1 & flp-2(gk1039)	52.34	46.51	0.06	0.082	ns	321	744	PS7378[g]
flp-3(ok3265)	36.27	46.51	-0.10	0.013	ns	193	744	PS7379[g]
flp-6(ok3056)	88.36	72.27	0.16	0.000	****	292	743	VC2324
flp-7(ok2625)	50.84	56.50	-0.06	0.032	ns	419	1954	RB1990
flp-8(pk360)	24.19	85.51	-0.61	0.000	****	124	283	PT501[i]
flp-10(ok2624)	30.08	46.51	-0.16	0.001	*	123	744	RB1989
flp-11(tm2706)	43.02	72.27	-0.29	0.000	****	172	743	FX02706
flp-12(ok2409)	35.29	40.73	-0.05	0.294	ns	102	960	RB1863
flp-13 (tm2427)	44.21	47.96	-0.04	0.475	ns	190	196	PS6813[g]
flp-17(n4894)	20.47	40.73	-0.20	0.000	****	215	960	MT15933[i]
flp-18(db99)	90.11	54.39	0.35	0.000	****	91	706	AX1410[i]
flp-20(ok2964)	30.43	40.73	-0.10	0.058	ns	92	960	RB2188
flp-21(ok889)	52.38	56.50	-0.04	0.114	ns	462	1954	RB982
flp-21(pk1601)	20.57	56.50	-0.36	0.000	****	982	1954	AX1129[f]
flp-21(sy880)	29.79	47.96	-0.18	0.004	ns	94	196	PS7371[e]
flp-25(gk1016)	56.40	72.27	-0.16	0.000	****	344	743	VC1982
flp-26(gk3015)	45.06	72.27	-0.27	0.000	****	162	743	VC3017
flp-32(sy853)	38.18	49.03	-0.10	0.128	ns	55	1185	PS7219[h]
flp-34 (ok3071)	47.92	49.03	-0.01	0.882	ns	48	1185	PS7221[g]
flp-34 (sy810)	67.33	49.03	0.18	0.001	*	101	1185	PS7220[g]
flp-34 (sy811)	67.86	49.03	0.18	0.006	ns	56	1185	PS7279[f]

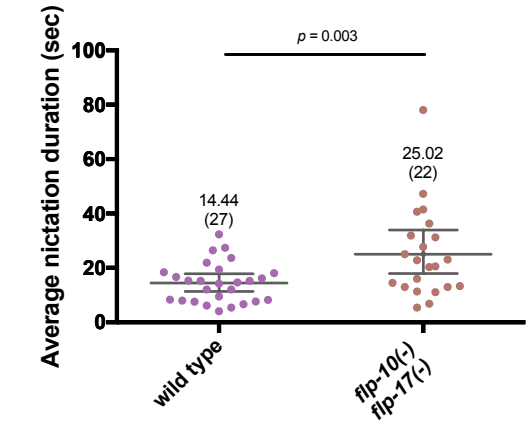

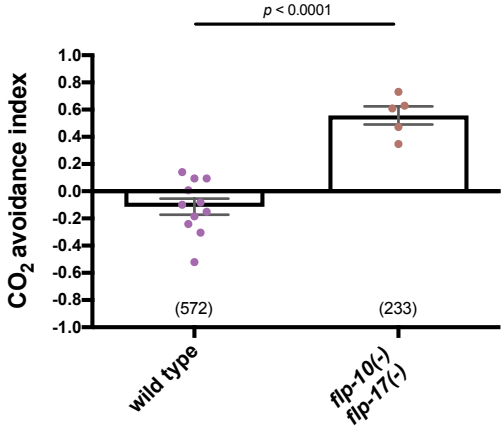

Figure 2.9. FMRFamide-like peptides are coordinately up-regulated during dauer development. (A) Fold changes in gene expression for all 118 *C. elegans* neuropeptide genes. Closed and open circles indicate significant and non-significant differential expression, respectively. The most up- and down-regulated genes of each family are labeled for reference. (B) Average Spearman correlation scores of genes to other genes of the same neuropeptide family, calculated across our RNA-seq dataset. Indicated is the bootstrapped mean and 99% confidence interval. (C) Survey for *flp* genes involved in the dauer entry decision. Footnotes: a−mean percentage calculated by nonparametric bootstrapping. b−the mean difference in dauer entry probability between wild type and mutant animals, calculated using Bayesian probability. c−calculated via permutation test. d−determined using a cutoff of Bonferroni-corrected p-value < 0.05: ****$p < 0.0001$, *$p < 0.05$, ns, not significant. e to j−strains outcrossed 1, 2, 3, 4, >4 and 6 times, respectively. (D-E) Nictation duration (D) and CO_2 avoidance (E) assays.

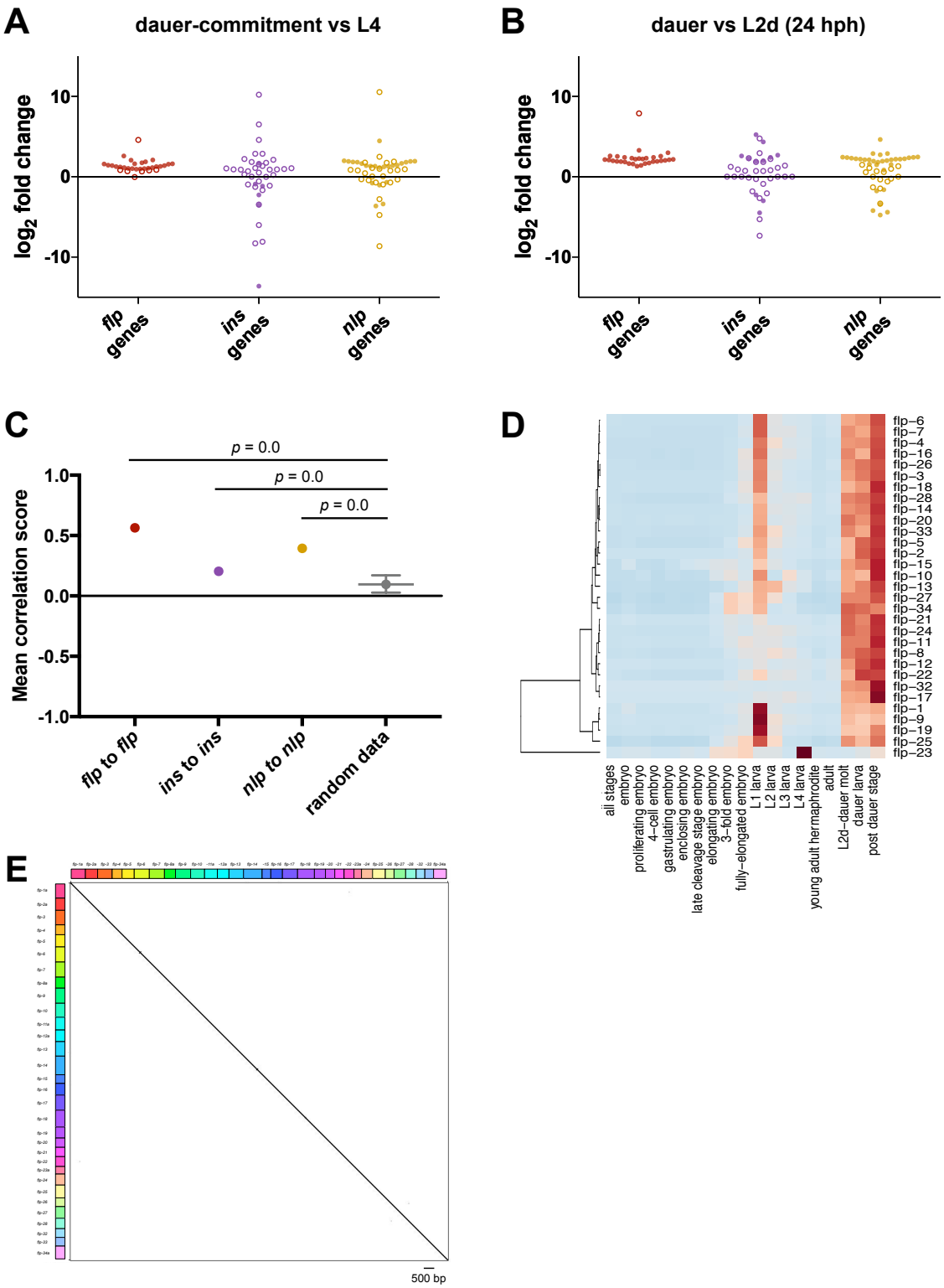
A
dauer-commitment vs L4
log2 fold change
10
0
-10
flp genes
ins genes
nlp genes
B
dauer vs L2d (24 hph)
log2 fold change
10
0
-10
flp genes
ins genes
nlp genes
C
p = 0.0
p = 0.0
p = 0.0
Mean correlation score
1.0
0.5
0.0
-0.5
-1.0
flp to flp
ins to ins
nlp to nlp
random data
D
flp–6
flp–7
flp–4
flp–16
flp–26
flp–3
flp–18
flp–28
flp–14
flp–20
flp–33
flp–5
flp–2
flp–15
flp–10
flp–13
flp–27
flp–34
flp–21
flp–24
flp–11
flp–8
flp–12
flp–22
flp–32
flp–17
flp–1
flp–9
flp–19
flp–25
flp–23
all stages
embryo
proliferating embryo
4–cell embryo
gastrulating embryo
enclosing embryo
late cleavage stage embryo
elongating embryo
3–fold embryo
fully–elongated embryo
L1 larva
L2 larva
L3 larva
L4 larva
young adult hermaphrodite
adult
L2d–dauer molt
dauer larva
post dauer stage
E
500 bp

Figure 2.10. FMRFamide-like peptides are coordinately up-regulated during dauer development. (A) Fold changes in gene expression for all 118 *C. elegans* neuropeptide genes during dauer-commitment versus L4 and (B) dauer versus L2d. Each circle represents an individual neuropeptide gene. Closed and open circles indicate significant and non-significant differential expression, respectively. (C) Average Spearman correlation scores of genes to other genes of the same neuropeptide family, calculated across 246 publically available RNA-seq datasets describing various *C. elegans* life stages and experimental conditions, including embryos, larvae, adults, and males (6). (D) Heatmap of *flp* median gene expression (analyzed in TPM) across the 246 RNA-seq datasets (6). The expression data was scaled and heatmapped as in Figure 3. (E) Dotplot of the coding sequences of all 31 *flp* genes, compared against each other. The x- and y-axes represent the concatenated coding sequences of the 31 *flp* genes (using only the a isoform, if multiple isoforms exist for that gene). Regions of sequence similarity are represented as a diagonal line of hits along the alignment space, and a minimum of 20 identical, consecutive nucleotides were required to generate a hit.

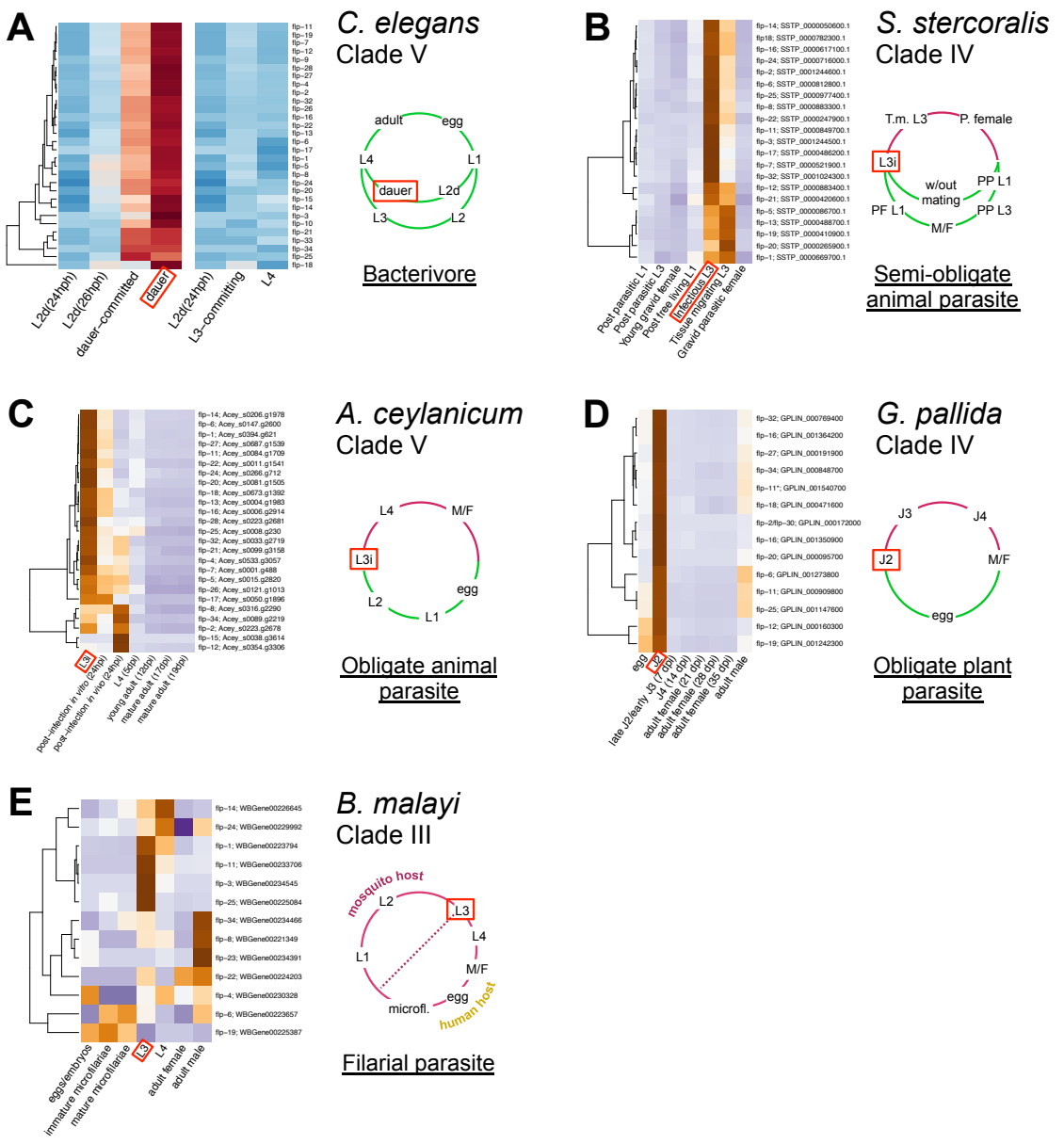

Figure 2.11. FMRFamide-like peptides are coordinately up-regulated in host-seeking infective juveniles of parasitic nematodes. The life cycle and clade membership (out of five major clades of Nematoda (108)) of each species are indicated to the right of each heatmap. Green life cycle regions indicate stages that are free-living or external to a host. Red life cycle regions indicate stages internal to a host. The dauer and infective juvenile stages are highlighted in red boxes. (A) Expression of *flp* genes in the free-living

C. elegans (from our data). Red and blue indicate high and low expression scores, respectively. (B-E) Expression of *flp* orthologs/analogs in the transcriptomes of (B) the semi-obligate animal parasite *Strongyloides stercoralis*, (C) the obligate animal parasite *Ancylostoma ceylanicum*, (D) the obligate plant parasite *Globodera pallida*, and (E) the filarial parasite *Brugia malayi*. Orange and purple indicate high and low expression scores, respectively. Transcriptomic data from (70-73). Abbreviations are PP: post-parasitic, M/F: adult male and female, PF: post-free-living, T.m.: tissue migrating, P. female: parasitic female.

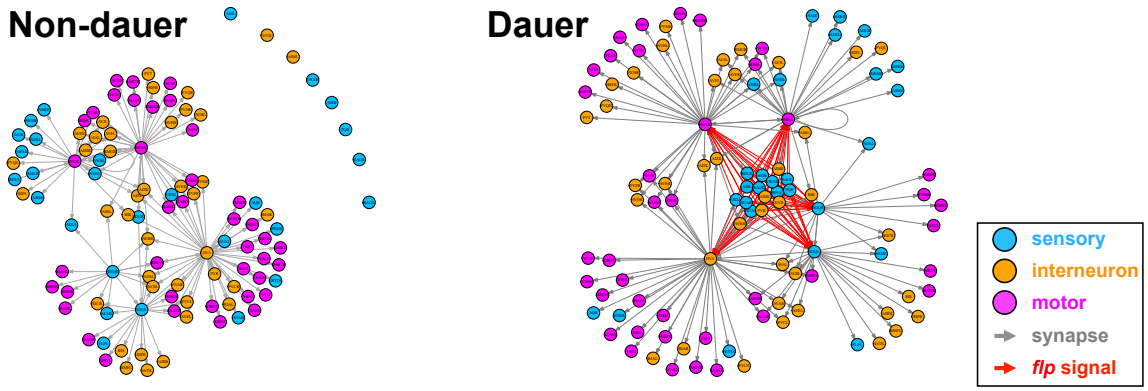

Figure 2.12. Model of circuit changes during dauer development via non-synaptic FLP signaling. The FLP-10 ligand EGL-6 receptor circuit is shown as an example. The synaptic connections that are indicated are (in pre-synaptic to post-synaptic order) from *flp-10* expressing neurons to *egl-6* expressing neurons to directly downstream synaptic targets. Expression pattern, connectomic, and biochemical data was used from (7-9), WormWiring, and WormBase.

2.7 References

1. McLaughlin KA*, et al.* (2015) Causal effects of the early caregiving environment on development of stress response systems in children. *Proceedings of the National Academy of Sciences of the United States of America* 112(18):5637-5642.

2. McQuaid RJ, McInnis OA, Stead JD, Matheson K, & Anisman H (2013) A paradoxical association of an oxytocin receptor gene polymorphism: early-life adversity and vulnerability to depression. *Frontiers in neuroscience* 7:128.

3. Reichmann F & Holzer P (2016) Neuropeptide Y: A stressful review. *Neuropeptides* 55:99-109.

4. Teicher MH, Samson JA, Anderson CM, & Ohashi K (2016) The effects of childhood maltreatment on brain structure, function and connectivity. *Nat Rev Neurosci* 17(10):652-666.

5. Gilbert SF (2000) Developmental Biology. (Sinauer Associates, Sunderland (MA)).

6. Fusco G & Minelli A (2010) Phenotypic plasticity in development and evolution: facts and concepts. Introduction. *Philosophical transactions of the Royal Society of London. Series B, Biological sciences* 365(1540):547-556.

7. Janzen FJ & Phillips PC (2006) Exploring the evolution of environmental sex determination, especially in reptiles. *J Evol Biol* 19(6):1775-1784.

8. Woodward DE & Murray JD (1993) On the effect of temperature-dependent sex determination on sex ratio and survivorship in crocodilians. *Proceedings of the Royal Society of London. Series B: Biological Sciences* 252(1334):149.

9. Newman RA (1992) Adaptive plasticity in amphibian metamorphosis. *BioScience* 42(9):671-678.

10. Cassada RC & Russell RL (1975) The dauerlarva, a post-embryonic developmental variant of the nematode *Caenorhabditis elegans*. *Developmental biology* 46(2):326-342.

11. Fielenbach N & Antebi A (2008) *Caenorhabditis elegans* dauer formation and the molecular basis of plasticity. *Genes & development* 22(16):2149-2165.

12. Golden JW & Riddle DL (1984) The *Caenorhabditis elegans* dauer larva: developmental effects of pheromone, food, and temperature. *Developmental biology* 102(2):368-378.

13. Schaedel ON, Gerisch B, Antebi A, & Sternberg PW (2012) Hormonal signal amplification mediates environmental conditions during development and controls an irreversible commitment to adulthood. *PLoS biology* 10(4):e1001306.

14. Wadsworth WG & Riddle DL (1989) Developmental regulation of energy metabolism in *Caenorhabditis elegans*. *Developmental biology* 132(1):167-173.

15. Oriordan VB & Burnell AM (1990) Intermediary metabolism in the dauer larva of the nematode *Caenorhabditis-Elegans*. 2. The Glyoxylate Cycle and Fatty-Acid Oxidation. *Comp Biochem Phys B* 95(1):125-130.

16. Albert PS & Riddle DL (1983) Developmental alterations in sensory neuroanatomy of the *Caenorhabditis elegans* dauer larva. *The Journal of comparative neurology* 219(4):461-481.

17. Schroeder NE*, et al.* (2013) Dauer-specific dendrite arborization in *Caenorhabditis elegans* is regulated by KPC-1/Furin. *Current Biology* 23(16):1527-1535.

18. Hallem EA*, et al.* (2011) A sensory code for host seeking in parasitic nematodes. *Current biology : CB* 21(5):377-383.

19. Lee H*, et al.* (2012) Nictation, a dispersal behavior of the nematode *Caenorhabditis elegans*, is regulated by IL2 neurons. *Nature neuroscience* 15(1):107-112.

20. Vanfleteren JR & Braeckman BP (1999) Mechanisms of life span determination in *Caenorhabditis elegans*. *Neurobiol Aging* 20(5):487-502.

21. Klass M & Hirsh D (1976) Non-ageing developmental variant of *Caenorhabditis elegans*. *Nature* 260(5551):523-525.

22. Erkut C*, et al.* (2013) Molecular strategies of the *Caenorhabditis elegans* dauer larva to survive extreme desiccation. *PloS one* 8(12):e82473.

23. Gerstein MB*, et al.* (2010) Integrative analysis of the *Caenorhabditis elegans* genome by the modENCODE project. *Science* 330(6012):1775-1787.

24. Wang J & Kim SK (2003) Global analysis of dauer gene expression in *Caenorhabditis elegans*. *Development* 130(8):1621-1634.

25. Karp X (2016) Working with dauer larvae. *WormBook : the online review of Caenorhabditis elegans biology*:1-19.

26. Husson SJ & Schoofs L (2007) Altered neuropeptide profile of *Caenorhabditis elegans* lacking the chaperone protein 7B2 as analyzed by mass spectrometry. *FEBS letters* 581(22):4288-4292.

27. Li C & Kim K (2014) Family of FLP peptides in *Caenorhabditis elegans* and related nematodes. *Frontiers in endocrinology* 5:150.

28. Pierce SB*, et al.* (2001) Regulation of DAF-2 receptor signaling by human insulin and *ins-1*, a member of the unusually large and diverse *Caenorhabditis elegans* insulin gene family. *Genes & development* 15(6):672-686.

29. Jia K, Albert PS, & Riddle DL (2002) DAF-9, a cytochrome P450 regulating *Caenorhabditis elegans* larval development and adult longevity. *Development* 129(1):221-231.

30. Motola DL*, et al.* (2006) Identification of ligands for DAF-12 that govern dauer formation and reproduction in *Caenorhabditis elegans*. *Cell* 124(6):1209-1223.

31. Gerisch B, Weitzel C, Kober-Eisermann C, Rottiers V, & Antebi A (2001) A hormonal signaling pathway influencing *Caenorhabditis elegans* metabolism, reproductive development, and life span. *Developmental cell* 1(6):841-851.

32. Sulston JE & Horvitz HR (1977) Post-embryonic cell lineages of the nematode, *Caenorhabditis elegans*. *Developmental biology* 56(1):110-156.

33. Marinov GK*, et al.* (2014) From single-cell to cell-pool transcriptomes: stochasticity in gene expression and RNA splicing. *Genome research* 24(3):496-510.

34. Miura F*, et al.* (2008) Absolute quantification of the budding yeast transcriptome by means of competitive PCR between genomic and complementary DNAs. *BMC genomics* 9:574.

35. Aken BL*, et al.* (2016) The Ensembl gene annotation system. *Database (Oxford)* 2016.

36. Howe KL*, et al.* (2016) WormBase 2016: expanding to enable helminth genomic research. *Nucleic Acids Res* 44(D1):D774-780.

37. Anders S & Huber W (2010) Differential expression analysis for sequence count data. *Genome biology* 11(10):R106.

38. Anders S*, et al.* (2013) Count-based differential expression analysis of RNA sequencing data using R and Bioconductor. *Nat Protoc* 8(9):1765-1786.

39. Jones SJ*, et al.* (2001) Changes in gene expression associated with developmental arrest and longevity in *Caenorhabditis elegans*. *Genome research* 11(8):1346-1352.

40. Futschik ME & Carlisle B (2005) Noise-robust soft clustering of gene expression time-course data. *J Bioinform Comput Biol* 3(4):965-988.

41. Kumar L & M EF (2007) Mfuzz: a software package for soft clustering of microarray data. *Bioinformation* 2(1):5-7.

42. Kanehisa M, Furumichi M, Tanabe M, Sato Y, & Morishima K (2017) KEGG: new perspectives on genomes, pathways, diseases and drugs. *Nucleic Acids Res* 45(D1):D353-D361.

43. Kanehisa M & Goto S (2000) KEGG: kyoto encyclopedia of genes and genomes. *Nucleic Acids Res* 28(1):27-30.

44. Kanehisa M, Sato Y, Kawashima M, Furumichi M, & Tanabe M (2016) KEGG as a reference resource for gene and protein annotation. *Nucleic Acids Res* 44(D1):D457-462.

45. Mi H*, et al.* (2017) PANTHER version 11: expanded annotation data from Gene Ontology and Reactome pathways, and data analysis tool enhancements. *Nucleic Acids Res* 45(D1):D183-D189.

46. Kaplan F*, et al.* (2011) Ascaroside expression in *Caenorhabditis elegans* is strongly dependent on diet and developmental stage. *PloS one* 6(3):e17804.

47. von Reuss SH*, et al.* (2012) Comparative metabolomics reveals biogenesis of ascarosides, a modular library of small-molecule signals in C. elegans. *J Am Chem Soc* 134(3):1817-1824.

48. Li C & Kim K (2008) Neuropeptides. *WormBook : the online review of C. elegans biology*:1-36.

49. Cohen M*, et al.* (2009) Coordinated regulation of foraging and metabolism in *Caenorhabditis elegans* by RFamide neuropeptide signaling. *Cell metabolism* 9(4):375-385.

50. Lee D, Lee H, Kim N, Lim DS, & Lee J (2017) Regulation of a hitchhiking behavior by neuronal insulin and TGF-beta signaling in the nematode *Caenorhabditis elegans*. *Biochem Biophys Res Commun* 484(2):323-330.

51. Braeckman BP, Houthoofd K, & Vanfleteren JR (2009) Intermediary metabolism. *WormBook : the online review of Caenorhabditis elegans biology*:1-24.

52. Ghosh S & Sternberg PW (2014) Spatial and molecular cues for cell outgrowth during *Caenorhabditis elegans* uterine development. *Developmental biology* 396(1):121-135.

53. Gupta BP, Hanna-Rose W, & Sternberg PW (2012) Morphogenesis of the vulva and the vulval-uterine connection. *WormBook : the online review of Caenorhabditis elegans biology*:1-20.

54. L'Hernault SW (2006) Spermatogenesis. *WormBook : the online review of Caenorhabditis elegans biology*:1-14.

55. Hobert O (2013) The neuronal genome of *Caenorhabditis elegans*. *WormBook : the online review of Caenorhabditis elegans biology*:1-106.

56. Kim Y, Bark S, Hook V, & Bandeira N (2011) NeuroPedia: neuropeptide database and spectral library. *Bioinformatics* 27(19):2772-2773.

57. Lindberg I, Tu B, Muller L, & Dickerson IM (1998) Cloning and functional analysis of *Caenorhabditis elegans* 7B2. *DNA and cell biology* 17(8):727-734.

58. Sieburth D*, et al.* (2005) Systematic analysis of genes required for synapse structure and function. *Nature* 436(7050):510-517.

59. Shen LL, Wang Y, & Wang DY (2007) Involvement of genes required for synaptic function in aging control in *Caenorhabditis elegans*. *Neuroscience bulletin* 23(1):21-29.

60. Kiontke K & Sudhaus W (2006) Ecology of *Caenorhabditis* species. *WormBook : the online review of Caenorhabditis elegans biology*:1-14.

61. Felix MA & Braendle C (2010) The natural history of *Caenorhabditis elegans*. *Current biology : CB* 20(22):R965-969.

62. Hallem EA & Sternberg PW (2008) Acute carbon dioxide avoidance in *Caenorhabditis elegans*. *Proceedings of the National Academy of Sciences of the United States of America* 105(23):8038-8043.

63. Krumsiek J, Arnold R, & Rattei T (2007) Gepard: a rapid and sensitive tool for creating dotplots on genome scale. *Bioinformatics* 23(8):1026-1028.

64. Smith ES, Martinez-Velazquez L, & Ringstad N (2013) A chemoreceptor that detects molecular carbon dioxide. *Journal of Biological Chemistry* 288(52):37071-37081.

65. Kim K & Li C (2004) Expression and regulation of an FMRFamide-related neuropeptide gene family in *Caenorhabditis elegans*. *J Comp Neurol* 475(4):540-550.

66. Ringstad N & Horvitz HR (2008) FMRFamide neuropeptides and acetylcholine synergistically inhibit egg-laying by *Caenorhabditis elegans*. *Nature neuroscience* 11(10):1168-1176.

67. Viney ME (2009) How did parasitic worms evolve? *BioEssays : news and reviews in molecular, cellular and developmental biology* 31(5):496-499.

68. Okumura E & Yoshiga T (2014) Host orientation using volatiles in the phoretic nematode *Caenorhabditis japonica*. *J Exp Biol* 217(18):3197-3199.

69. McCoy CJ*, et al.* (2014) New insights into the FLPergic complements of parasitic nematodes: informing deorphanisation approaches. *EuPA open proteomics* 3:262-272.

70. Choi YJ*, et al.* (2011) A deep sequencing approach to comparatively analyze the transcriptome of lifecycle stages of the filarial worm, *Brugia malayi*. *PLoS neglected tropical diseases* 5(12):e1409.

71. Cotton JA*, et al.* (2014) The genome and life-stage specific transcriptomes of *Globodera pallida* elucidate key aspects of plant parasitism by a cyst nematode. *Genome biology* 15(3):R43.

72. Schwarz EM*, et al.* (2015) The genome and transcriptome of the zoonotic hookworm *Ancylostoma ceylanicum* identify infection-specific gene families. *Nature genetics* 47(4):416-422.

73. Stoltzfus JD, Minot S, Berriman M, Nolan TJ, & Lok JB (2012) RNAseq analysis of the parasitic nematode *Strongyloides stercoralis* reveals divergent regulation of canonical dauer pathways. *PLoS neglected tropical diseases* 6(10):e1854.

74. Bain O & Babayan S (2003) Behaviour of filariae: morphological and anatomical signatures of their life style within the arthropod and vertebrate hosts. *Filaria journal* 2(1):16.

75. Felix MA & Duveau F (2012) Population dynamics and habitat sharing of natural populations of *Caenorhabditis elegans* and *C. briggsae*. *BMC biology* 10:59.

76. Nusbaum MP, Blitz DM, Swensen AM, Wood D, & Marder E (2001) The roles of co-transmission in neural network modulation. *Trends in neurosciences* 24(3):146-154.

77. Salio C, Lossi L, Ferrini F, & Merighi A (2006) Neuropeptides as synaptic transmitters. *Cell Tissue Res* 326(2):583-598.

78. Landgraf R & Neumann ID (2004) Vasopressin and oxytocin release within the brain: a dynamic concept of multiple and variable modes of neuropeptide communication. *Frontiers in neuroendocrinology* 25(3-4):150-176.

79. Bargmann CI (2012) Beyond the connectome: how neuromodulators shape neural circuits. *BioEssays : news and reviews in molecular, cellular and developmental biology* 34(6):458-465.

80. Jekely G (2013) Global view of the evolution and diversity of metazoan neuropeptide signaling. *Proceedings of the National Academy of Sciences of the United States of America* 110(21):8702-8707.

81. Dockray GJ (2004) The expanding family of -RFamide peptides and their effects on feeding behaviour. *Experimental physiology* 89(3):229-235.

82. Elphick MR & Mirabeau O (2014) The evolution and variety of RFamide-type neuropeptides: insights from deuterostomian invertebrates. *Frontiers in endocrinology* 5:93.

83. Cardoso JC, Felix RC, Fonseca VG, & Power DM (2012) Feeding and the rhodopsin family g-protein coupled receptors in nematodes and arthropods. *Frontiers in endocrinology* 3:157.

84. Guillermin ML, Castelletto ML, & Hallem EA (2011) Differentiation of carbon dioxide-sensing neurons in *Caenorhabditis elegans* requires the ETS-5 transcription factor. *Genetics* 189(4):1327-1339.

85. White JG, Southgate E, Thomson JN, & Brenner S (1986) The structure of the nervous system of the nematode *Caenorhabditis elegans*. *Philosophical transactions of the Royal Society of London. Series B, Biological sciences* 314(1165):1-340.

86. Dalzell JJ, McMaster S, Fleming CC, & Maule AG (2010) Short interfering RNA-mediated gene silencing in *Globodera pallida* and *Meloidogyne incognita* infective stage juveniles. *International journal for parasitology* 40(1):91-100.

87. Morris R*, et al.* (2017) A neuropeptide modulates sensory perception in the entomopathogenic nematode *Steinernema carpocapsae*. *PLoS Pathog* 13(3):e1006185.

88. Sudhaus W (2010) Preadaptive plateau in Rhabditida (Nematoda) allowed the repeated evolution of zooparasites, with an outlook on evolution of life cycles within Spiroascarida. *Palaeodiversity* 3, Supplement:117-130.

89. De Ley P (2006) A quick tour of nematode diversity and the backbone of nematode phylogeny. *WormBook : the online review of Caenorhabditis elegans biology*:1-8.

90. Han Z, Boas S, & Schroeder NE (2015) Unexpected variation in neuroanatomy among diverse nematode species. *Front Neuroanat* 9:162.

91. Brenner S (1974) The genetics of *Caenorhabditis elegans*. *Genetics* 77(1):71-94.

92. Mello C & Fire A (1995) DNA transformation. *Methods in cell biology* 48:451-482.

93. Maduro M & Pilgrim D (1995) Identification and cloning of *unc-119,* a gene expressed in the *Caenorhabditis elegans* nervous system. *Genetics* 141(3):977-988.

94. Arribere JA*, et al.* (2014) Efficient marker-free recovery of custom genetic modifications with CRISPR/Cas9 in *Caenorhabditis elegans*. *Genetics* 198(3):837-846.

95. Wickham H (2009) *ggplot2: Elegant Graphics for Data Analysis* (Springer-Verlag New York).

96. Yu G, Wang LG, Han Y, & He QY (2012) clusterProfiler: an R package for comparing biological themes among gene clusters. *OMICS* 16(5):284-287.

97. Warnes GR*, et al.* (2016) gplots: Various R programming tools for plotting data.

98. Neuwirth E (2014) RColorBrewer: ColorBrewer Palettes. R package version 1.1-2.

99. Jones E, Oliphant T, & Peterson P (2001) SciPy: open source scientific tools for Python.

100. Bray NL, Pimentel H, Melsted P, & Pachter L (2016) Near-optimal probabilistic RNA-seq quantification. *Nature biotechnology* 34(5):525-527.

101. Pachter L (2011) Models for transcript quantification from RNA-Seq. *arXiv*. eprint arXiv:1104.3889(eprint arXiv:1104.3889):eprint arXiv:1104.3889.

102. Golden JW & Riddle DL (1984) A pheromone-induced developmental switch in *Caenorhabditis elegans*: Temperature-sensitive mutants reveal a wild-type temperature-dependent process. *Proceedings of the National Academy of Sciences of the United States of America* 81(3):819-823.

103. Efron B & Tibshirani RJ (1994) *An introduction to the bootstrap* (CRC press).

104. Sivia DS & Skilling J (2006) *Data analysis: a Bayesian tutorial* (Oxford University Press).

105. Jones E, Oliphant T, & Peterson P (2001) SciPy: open source scientific tools for Python.

106. Bargmann CI, Hartwieg E, & Horvitz HR (1993) Odorant-selective genes and neurons mediate olfaction in *Caenorhabditis elegans*. *Cell* 74(3):515-527.

107. McVeigh P*, et al.* (2005) Analysis of FMRFamide-like peptide (FLP) diversity in phylum Nematoda. *International journal for parasitology* 35(10):1043-1060.

108. Blaxter M & Koutsovoulos G (2015) The evolution of parasitism in Nematoda. *Parasitology* 142 Suppl 1:S26-39.